Hydrometeorological study applied to the Buena Vista del Cobre mine spillage in 2014, in the Sonora River Basin

Author:

Supervisor: UMA

Mentors: , IHE Delft

ACKNOWLEDGMENTS

Finally, to my family, who have always encouraged me to pursue my goals. Especially my mother, who has instilled values in me and has always supported my decisions.

Abstract

The Sonora Basin is located in the central-northern zone of the homonymous state, north of the Mexican Republic. On August 6, 2014, approximately 40,000 m^3 of coper-rich solution containing ions and colloids of Potentially Toxic Elements (PTE), including heavy metals, spilt into the Tinajas stream in the Municipality of Cananea (Sonora). The acidic solution was stored in a dam belonging to the Buena Vista del Cobre Company (BVC), a subsidiary of Grupo México. The following thesis aims to determine whether the spill was due to heavy rainfall caused by a hurricane or whether another factor was responsible for the incident. In addition, future rainfall trends will be analysed. In order to find out by means of experiments whether it is possible that after the construction of two new dams an incident like the one in 2014 will occur again.

Key words: spillage, Sonora River Basin, hydrometeorology.

Contents

1. Introduction

1.1. Justification and background.

This document has been prepared as a thesis for the 15th edition of the Master's Degree in Water Resources and the Environment (RHYMA), carried out at the Institute for Water Education (IHE), in Delft, the Netherlands. Its tutors are Dr. Jose Manuel Gil Marquez, UMA Department of Geology and Ecology, Dr. Jochen Wenninger and Dr. Konstantina Katsanou, IHE Delft Department of Water Resources and Ecosystems.

This thesis is part of a project located in the Sonora River Catchment in Mexico funded by Grupo Mexico, which aims to analyse the hydrology of the Sonora River basin and the potential impacts of the mining activity in the area.

The Sonora Basin is located in the central-northern zone of the homonymous state, north of the Mexican Republic, more specifically within the coordinates 29° 22' - 31° 01' north latitude and at 109° 75' - 110° 67' west longitude (Figure 1). Historically it is a mining region, with copper extraction being the main economic activity in the area.

On August 6, 2014, approximately 40,000 m3 of coper-rich solution containing ions and colloids of Potentially Toxic Elements (PTE), including heavy metals, spilt into the Tinajas stream in the Municipality of Cananea (Sonora). The acidic solution was stored in a dam belonging to the Buena Vista del Cobre Company (BVC), a subsidiary of Grupo México.

The environmental authorities indicated that the spillage affected the Tinajas Stream (17.6 km) which flows into the Bacanuchi River (64 km), which in turn joins the Sonora River (190 km) that drains to the El Molinito Reservoir (Fig. 2). In this case, the contaminant travelled 140 km and didn’t reached El Molinito Reservoir, on August 10, while from August 11th the effect of the spillage started to reduce.

The aim of this study is to determine the likelihood of a new spillage by the BVC mine. To find out whether the measures taken by the mining company are sufficient to stop extreme rainfall events and to avoid heavy metal contamination.

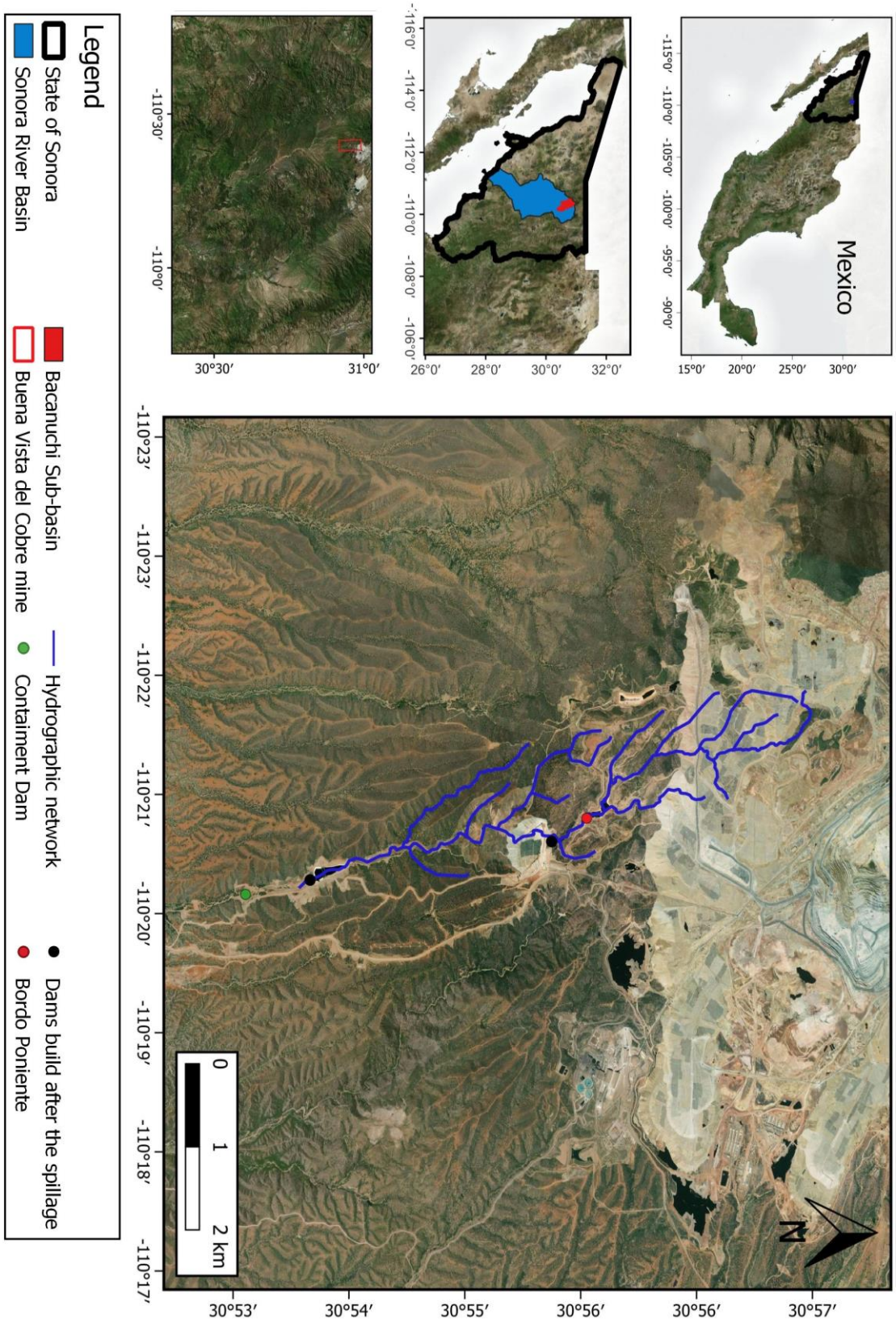

Figure 1. Location of the study area.

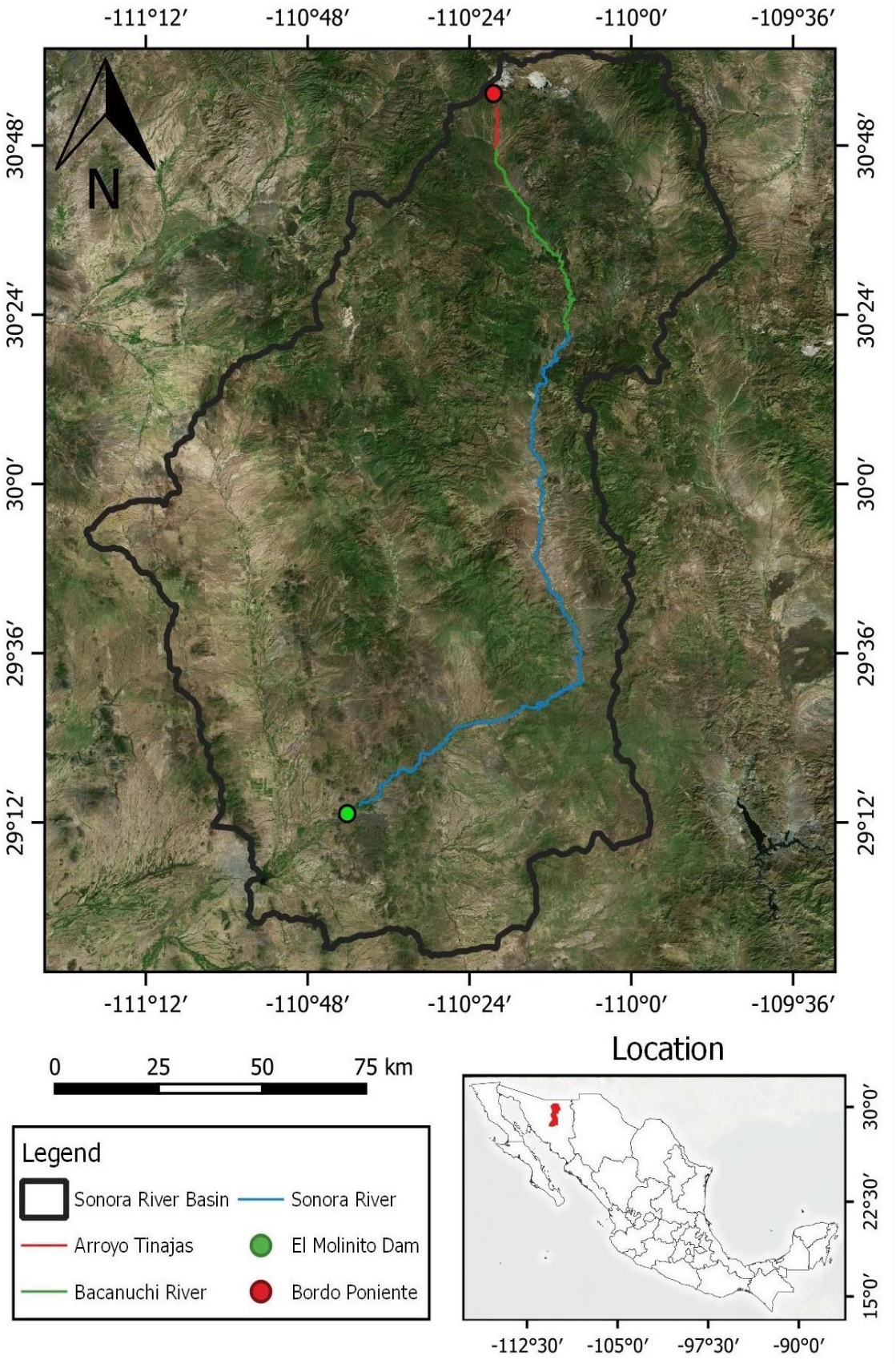

Figure 2. The main stream of the Sonora River, Bacanuchi River and Tinajas Stream.

In response, the BVC technicians carried out a series of emergency actions in an attempt to reduce the impact of the spillage. First, they built a dam that managed to retain approximately 2,366 m^3 of acid solution (Fig. 1) and carried out an intensive neutralisation campaign, adding lime slurries to the affected water. Later, the contaminated materials visually identified along the river were collected and disposed of within the company's land.

To identify any long-lasting impacts of this event, a project was initiated which among others aims to analyse the behaviour of the hydrology of the Sonora River basin.

The focus of this thesis is the analysis of rainfall time series, both past and future, and its impact on the Bordo Poniente Dam. In addition, climate change's effect on the dam will be analysed, as well as with the later built dams, downstream in the Tinajas Stream.

1.2. Objectives and Research Questions:

The overall objective of this thesis is to carry out a preliminary water resource assessment of the Sonora River Basin and to analyse the long-term and seasonal historical and future precipitation behaviour.

The specific objectives are to:

i. collect hydro-meteorological information from ground stations (CONAGUA), satellite databases (CHIRPS), and climate change projections to provide hydrological and meteorological background information before, during, and after the spillage event of 6th August 2014 at the Buenavista del Cobre Mine, and describe the hydrological conditions.
ii. Assess the potential effects of climatic changes on the recurrence of extreme rainfall events and the water resources in the catchment.
iii. Evaluate potential risks emerging from changed precipitation pattern on the mine reservoirs.

1.3. Literature Review

To better understand the situation prior to the incident, the following studies have been consulted: *Estudio de la contaminación por metales pesados en el río Sonora y su afluente el río Bacanuchi* (Yocupicio Anaya, 1987); *Introducción al estudio hidrogeográfico y balance hidrológico de la cuenca del río Sonora hasta la estación hidrométrica "El Oregano"* (Infante Blanco, 1998) and *Evaluación hidrológica superficial de la cuenca del río Sonora* (Navarro Apodaca, 2009). The first consists of a study of heavy metal contamination in the Sonora River and its tributary, the Bacanuchi River. The other two theses confirm the aridity of the Sonora river basin and calculate the parameters that influence the surface hydrology of the Sonora river basin as well as its sub-basins.

As a result of the spillage that occurred on August 6, 2014, theses and articles were written on the matter: *Modelización conjunta de los recursos hídricos superficiales y subterráneos de la cuenca alta del río Sonora* (Fajardo Calzada, 2016); *Evaluación de la*

Retencion de metales pesados en los carbonatos pedogénicos de los sedimentos en la cuenca del rio sonora (UNAM, 2016) and *Caracterización hidrogeológica de la subcuenca río Bacanuchi, Sonora, México* (Araujo Quintero, 2017).

The National Water Commission (CONAGUA) made a report on the 2014 spill. This report states that during the days immediately following the spill, there was an increase in the metal concentration along the river. Some metals such as aluminium, iron, manganese and barium may be of natural origin. The 'El Molinito' reseivour, was not affected by contamination from the acid solution.

Finally, reference should be made to the article Síntesis, análisis e interpretación de la información publicada sobre el derrame de unos 40,000 m^3 de solución ácida ferro-cuprífera de la Mina Buenavista del Cobre (García, 2022), which synthesizes the information published so far about the event.

2. Methodology

The following section describes the methodology that has been followed in the study of precipitation in the Sonora River Basin.

Meteorological data was obtained from available stations in the Sonora River Basin (CONAGUA, 2023). In total, rainfall information was downloaded from 22 stations located throughout the basin, despite the large number of stations only 4 of them, the closest to BVC, were used. A gap was identified in the data from 2015 onwards. To tackle this issue, satellite data was downloaded from the "Climate Hazards Group InfraRed Precipitation with Station data" (CHIRPS, 2023). This way a continuous record from 1981 to the present was obtained.

For future rainfall precipitation predictions, daily and monthly information was downloaded from the European Union's Earth Observation Program (Copernicus, 2023). More specifically from CMIP6 climate projection, where the historical climate series 1964-2014 and the future projections 2015-2049 of 5 different experiments could be obtained. Each experiment took into account 5 different Shared Socio-economic Pathaway (SSP) scenarios.

The double-mass curves method was used, to compare the data from the meteorological stations with the satellite information database (CHIRPS) and thus obtain a long and reliable series.

The double-mass curve analysis introduced by Kohler (1949) is a graphical method of identifying and adjusting inconsistencies in a station record by comparing its time trend with those of other stations. Changes in the slope of the double-mass curve reflect changes in exposure or location of the gauge, changes in the procedure of collecting and processing data, etc (WMO, 1994). The data collected from all the sites within the region should be highly correlated, have similar variability, and differ only by scaling factors and

random sampling variability. The homogeneity of the climatic time series was tested using the RAINBOW software tool (Raes, 2013).

This same methodology was used to compare the data from the Bacanuchi station with the other stations in the area to determine if these data were representative of the study area. The data from this station is used in the thesis because it is the closest station to BVC.

2.1. Frequency analysis and probability plotting

RAINBOW is a software tool designed to study agro-meteorological or hydrologic records which tests the homogeneity of the record by performing frequency analysis. The program is especially suitable for predicting the probability of exceedance of either low or high rainfall events, both of which are important parameters for the design and management of irrigation systems, drainage networks, and reservoirs.

2.1.1. Estimation of the probability of exceedance

The first step in the frequency analysis is the ranking of the rainfall data. After the rainfall data are ranked, a serial rank number (r) ranging from 1 to n (number of observations) is assigned. Subsequently, the probability that should be assigned to each of the rainfall heights has to be determined.

If the data is ranked in descending order, the highest value first and the lowest value last, the probability is an estimate of the likelihood that the corresponding rainfall depth will be exceeded. When data is ranked from the lowest to the highest value, the probability refers to the probability of non-exceedance. Hence the probabilities are estimates of cumulative probability. It is formed by summing the probabilities of occurrence of all events greater than (probability of exceedance) or less than (probability of non-exceedance) at some given rainfall height. Since these probabilities are unknown the probability of exceedance has to be estimated by one or another method. For this purpose the Weibull probability distribution was used (Weibul, 1939).

The Weibull distribution is commonly used for frequency analysis as well as risk and reliability analysis of the lifetimes of systems as well as their components. Its applications have been reported frequently in hydrology and meteorology.

The random variable x is reported to have a Weibull distribution if its probability density function (pdf) is given by Equation 1a:

$$f(x) = \frac{a}{b}\left(\frac{x}{b}\right)^{a-1} exp\left[-\left(\frac{x}{b}\right)^{a}\right], a > 0, b > 0. \quad \text{(Eq.1a)}$$

Its cumulative density function (cdf) can be expressed by Equation 1b:

$$F(x) = exp\left[-\left(\frac{x}{b}\right)^{a}\right], a > 0, b > 0. \quad \text{(Eq.1b)}$$

Where:

If a = 1, Equation (1a) is an exponential probability density function (pdf). Thus, the exponential distribution is a special case of the Weibull distribution. Moreover, this distribution can be generalised to the extreme value type-3 distribution by the transformation y = x - c, where c is a parameter.

2.1.2. Probability plot

A probability plot is a plot of the rainfall height versus their probabilities of exceedance as determined. When the data is plotted on arithmetic paper, where both axes have a linear scale, the data is not likely to be plotted on a straight line but rather follow a S-shaped curve. This plot is also called a percentage ogive.

If the data in a probability plot lie in a reasonable alignment, it may be assumed that the data can be approximated by the assumed distribution.

When probability plots are constructed and a line is drawn through the data, the tendency to extrapolate the data to extreme probabilities of exceedance is high. However, if the data do not follow the assumed distribution, the error in extrapolation can be quite large.

Probability plotting is an excellent graphical technique for testing distributional hypotheses. When the points in the probability plot do not fall in a logical alignment, the data is most likely not distributed as the selected distribution, especially if the points deviate from the straight line in some systematic manner. The extent and type of deviation from the assumed distribution may provide information about a more appropriate distribution. One can either recalibrate the distal axis of the probability plot or choose another distribution.

2.1.3. Estimating rainfall amounts for selected probabilities

The estimation of rainfall amounts for selected probabilities can be derived by graphic or numerical solution. In this case, the numerical solution was selected.

When annual rainfall is completely normally distributed the data in a probability plot will fall perfectly on the normal line. On this line the mean rainfall ($\bar{X}$) corresponds with the 50 per cent probability of exceedance, the $\bar{X} + s$ (standard deviation) corresponds with 15.87 % and the $\bar{X} - s$ with the 84.13% probability of exceedance (Raes, 2004). Since the normal distribution is completely characterised by its average and standard deviation, it can be used to estimate rainfall for selected probabilities or return periods:

$$X_p = \bar{X} \pm k\, s$$

Where:

X_p is the rainfall height having a specific probability of exceedance.

$\bar{X}$ is the sample mean, s the standard deviation, and k a frequency factor.

The sign and magnitude of the frequency factor vary according to the selected probability of exceedance.

2.1.4. Estimates of extreme rainfall (Gumbel distribution)

Estimates of extreme rainfall heights or intensities are required for the design of dams. Therefore, the annual maximum series, which is the set of maximum values observed during a period (minute(s), hour(s) or day(s)) in each year, is analysed. Several distribution functions can be selected to estimate extreme rainfall during the considered period. The Gumbel distribution which is skewed often gives satisfactory results (Chow et al., 1988).

The Extreme Value Type I (EVI) probability distribution function is given by the following equation:

$$F(x) = exp\left[-exp\left(\frac{x-u}{\propto}\right)\right] \qquad -\infty \leq x \leq \infty \tag{Eq.2a}$$

The parameters are estimated, by the following equation (Eqs. 2b and 2c):

$$\propto = \frac{\sqrt{6}s}{\pi} \tag{Eq.2b}$$

$$u = \bar{x} - 0.5772 \propto \tag{Eq.2c}$$

The parameter u is the mode of the distribution (point of maximum probability density). A reduced variate y can be defined as

$$y = \frac{x-u}{\propto} \tag{Eq.2d}$$

Substituting the reduced variate into Eq. 2a yields:

$$F(x) = exp[-exp(-y)] \tag{Eq.2e}$$

Solving for y:

$$y = -ln\left[ln\left(\frac{1}{F(x)}\right)\right] \tag{Eq.2f}$$

In the EVI distribution, the plot is a straight line, for large values of v, and also shows values of the return period T as an alternate axis to y,

$$\begin{aligned}\frac{1}{T} &= P(x \geq x_T) \\ &= 1 - P(x < x_T) \\ &= 1 - F(x_T)\end{aligned}$$

So,

$$F(x_T) = \frac{T-1}{T}$$

and, substituting into 2f,

$$y_T = -ln\left[ln\left(\frac{T}{T-1}\right)\right] \tag{Eq.2g}$$

For the EVI distribution, x_T is related to y_T by:

$$x_T = u + \propto y_T \quad \text{(Eq.2h)}$$

2.1.5. Intensity-Frequency-Duration Analysis

If rainfall data from a rain gauge is available for a long period such as 25 years or more, the frequency of occurrence of a given intensity can also be determined.

The entire rainfall record within a year is analysed to find the maximum intensities for various durations. Thus, each storm gives one value of maximum intensity for a given duration. The largest of all such values is taken to be the maximum intensity in that year for that duration. Likewise, the annual maximum intensity is obtained for different durations. Similar analysis yields the annual maximum intensities for various durations in different years. It will then be observed that the annual maximum intensity for any given duration is not the same every year, but it varies from year to year. In other words, it behaves as a random variable. So, if a 25-year record is available then there will be 25 values of the maximum intensity of any given duration, which constitute a sample of the random variable. These 25 values of any duration can be subjected to frequency analysis. Often the observed frequency distribution is well-fitted by a Gumbel distribution. Similar frequency analysis is carried out for other durations.

2.2. Pre-Spillage Precipitation Analysis

Pre-spillage precipitation analysis is applied to analyse the rainfall before the spillage on August 6, 2014. A water balance analysis was carried out, considering the portion of the basin that drains to Bordo Poniente Dam (SIATL, 2023). The objective is to find out if the rainfall events were enough to cause the spillage or if there was another cause.

For this water balance, previous rainfall, the percentage of precipitation that becomes run-off and the capacity of the Bordo Poniente Dam (120,000 m^3) will be taken into consideration in addition to the amount of previously stored water in the dam (40,000 m^3).

2.3. Trend analysis

To analyse the trend of both annual and seasonal extreme events XLSTAT program, a data analysis add-on for Microsoft Excel was used. Among all the options provided by this program, the Mann-Kendall trend analysis was applied.

The Mann-Kendall trend test analyses the difference in signs between earlier and later data points. The idea is that if a trend is present, the sign values will tend to increase constantly or decrease constantly.

The Mann–Kendall trend test (Mann, 1945; Kendall, 1975) is based on the correlation between the ranks of a time series and their time order. For a time series X = {x_1, x_2, ..., x_n}, the test statistic is given by the following equation:

$$S = \sum_{i<j} a_{ij} \quad \text{(Eq.3a)}$$

Where: $a_{ij} = sign(x_j - x_i) = sign(R_j - R_i) = \begin{cases} 1 & x_i < x_j \\ 0 & x_i = x_j \\ -1 & x_i = x_j \end{cases}$

(Eq.3b)

and Ri and Rj are the ranks of observations x_i and x_j of the time series, respectively. As can be seen from Equation 3b, the test statistic depends only on the ranks of the observations, rather than their actual values, resulting in a distribution-free test statistic. This is true because if data were to be transformed to any distribution, the ranks of the observations would remain the same. Distribution-free tests have the advantage that their power and significance are not affected by the actual distribution of the data. This is in contrast to parametric trend tests, such as the regression coefficient test, which assume that the data follow the Normal distribution and whose power can be greatly reduced in the case of skewed data (Yue et al., 2002).

Under the assumption that the data are independent and identically distributed, the mean and variance of the S statistic in Equation 3a above are given by Kendall 1975:

$$E(S) = 0 \quad \text{(Eq.3c)}$$

$$V_0(S) = n(n-1)(2n+5)/18 \quad \text{(Eq.3d)}$$

Where:

n is the number of observations.

The existence of tied ranks (equal observations) in the data results in a reduction of the variance of S.

$$V_0(S) = n(n-1)(2n+5)/18 - \sum_{j=1}^{m} t_j(t_j-1)(2t_j+5)/18 \quad \text{(Eq.3e)}$$

Where:

m is the number of groups of tied ranks, each with t_j tied observations.

Kendall (1975) also shows that the distribution of S tends to normality as the number of observations becomes large. The significance of trends can be tested by comparing the standardised variable u in Equation 3f with the standard normal variate at the desired significance level a, where the subtraction or addition of unity in Equation 3f is a continuity correction (Kendall, 1975). $u = \begin{cases} (S-1)/\sqrt{V_0(S)} & S > 0 \\ 0 & S = 0 \\ (S+1)/\sqrt{V_0(S)} & S < 0 \end{cases}$

(Eq.3f)

A trend analysis will be made of the number of extreme precipitation events at an annual basis. An analysis will also be made considering the seasonal rainfall for the same time period.

2.4. Global climate projection

Using future precipitation predictions, the behaviour of these climatic data series and the possible effect of future rainfall events on the Bordo Poniente Dam and the two new dams built to prevent future incidents will be analysed.

For this purpose, daily and monthly climate series were downloaded from the European Union's Earth Observation Program (Copernicus, 2023). More specifically from CMIP6 climate projection, where the historical climate series 1964-2014 and the future projections 2015-2049 of five different experiments could be obtained (Table 1). Each experiment considered five different scenarios.

Table 1. Experiments used in future projection analysis.

Experiment	Country
IPSL-CM6A-LR	France
EC-Earth-Veg-LR	European Union
CAMS-CSM1-0	China
GFDL-ESM4	USA
MRI-ESM2-0	Japan

The term "experiments" refers to the two main categories of CMIP6 simulations:

- Historical experiments which cover the period where modern climate observations exist. These experiments show how the Global Climate Models (GCMs) performs for the past climate and can be used as a reference period for comparison with scenario runs for the future. The period covered is typically 1850-2014.
- Climate projection experiments following the combined pathways of the Shared Socioeconomic Pathway (SSP) and Representative Concentration Pathway (RCP). The SSP scenarios provide different pathways for future climate forcing. The period covered is typically 2015-2100.

The SSPs describe alternative evolutions of future society in the absence of climate change or climate policy. SSPs 1 and 5 envision relatively optimistic trends for human development, with substantial investments in education and health, rapid economic growth, and well-functioning institutions. However, SSP5 assumes an energy-intensive, fossil-based economy, while in SSP1 there is an increasing shift toward sustainable practices. SSP3 and SSP4 envision more pessimistic development trends, with little investment in education or health, fast-growing population and increasing inequalities. In SSP3 countries prioritise regional security, whereas in SSP4 large inequalities within and across countries dominate, in both cases leading to societies that are highly vulnerable to climate change. SSP2 envisions a central pathway in which trends continue their historical patterns without substantial deviations (O'Neill et al., 2016).

The rows of the SSP forcing matrix shown in Figure 3 are defined by forcing pathways that achieve the same level of global average radiative forcing in 2100. The Scenario Model Intercomparison Project (ScenarioMIP) will carry out climate model simulations

for one particular land use and concentration pathway that leads to this level of radiative forcing. However, in principle, this forcing level can be achieved via pathways of emissions and land use that differ widely in terms of regional land use patterns, regional patterns of emissions of NTCFs (namely tropospheric aerosols, tropospheric O_3 precursors, and CH_4), and mixes of global emissions of greenhouse gases (GHGs) and NTCFs. For example, the different SSPs making up a given row of the matrix will have different patterns of regional economic growth, energy system development, air quality policies, land use, and other characteristics that will lead to the same global average forcing outcome being achieved by different means in each case. Thus, an open scientific question is the degree to which climate outcomes can be expected to differ between land use and emissions pathways that achieve the same global average radiative forcing level in 2100 but have different patterns of regional forcing.

In addition, the definition of global average forcing in 2100 includes the forcing effect of GHGs and NTCFs but excludes the biophysical effects of land use change on climate (e.g., through albedo or changes to the hydrological cycle). Thus, it is also an open question whether alternative pathways that achieve the same level of global average radiative forcing as defined here but differ in forcing due to the biophysical effects of land use change, would produce substantially different climate outcomes (O'Neil et al, 2016).

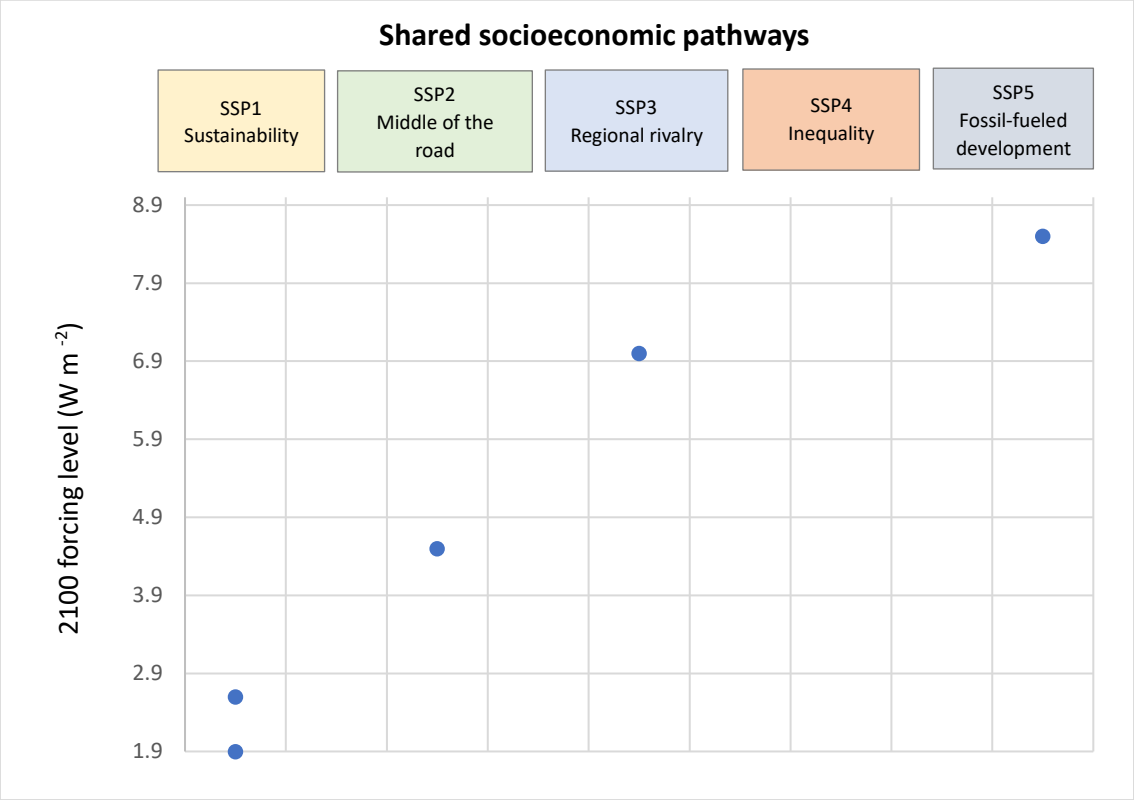

Figure 3. Characteristics of the 5 different scenarios considered in the climate projections experiments.

In order to be able to properly analyse the trends of the different experiments, it was decided to process the data using Statistical downscaling (SDS). This process allows us to homogenise the different scenarios, making the information representative of the study area. Statistical downscaling first derives statistical relationships between observed small-scale (often station-level) variables and larger-scale (GCM) variables, using either analogue methods (circulation typing), regression analysis, or neural network methods.

Statistical downscaling is the process of building an empirical model (Vasiliades et al., 2008):

$$y = F(x) \quad \text{(Eq. 4a)}$$

As predictands, y has been used as weather variables, such as monthly precipitation amounts. The predictor x has often been chosen as a characteristic of the weather circulation. If the function F is linear, Eq. 4a becomes

$$F(x) = ax + \varepsilon \quad \text{(Eq. 4b)}$$

with ε drawn from a normal distribution with zero mean and standard deviation σ, and $0<a<1$. The variations in ε are assumed to be independent from x. In this setting, the randomness in y stems from the randomness in ε. Hence, Eq. 4a must be understood as a stochastic equation (Von Storch, 1999).

Several statistical methods apply to the description of relationships between large-scale upper-air fields and local climate elements. Multiple linear regression (MLR), either based directly on grid point data or on principal components (PCs) of predictor fields, canonical correlation analysis (CCA), and non-linear methods such as multivariate splines and neural networks have been used most widely (Wilby and Wigley, 1997; Xu, 1999; Xu et al., 2005; Fowler et al., 2007). In this study, the GCM grid point outputs were downscaled using multiple regression equations between GCM predictor output variables and areal monthly precipitation. Stepwise screening of gridpoint data was found to be the best statistical model among canonical correlation analysis, singular value decomposition, and multiple regression models on principal components (PCs) of predictor fields for downscaling daily temperature in Europe (Huth, 1999). The predictors used in such analyses should be: a) well simulated by the GCM, b) strongly correlated with the predictand variable (precipitation), and c) available. Using these criteria, six predictor grid variables were used, namely the mean sea level pressure (mslp), the mean 2 m wind speed (swa), the precipitation (pcp), the mean surface temperature (st), the 500 hPa geopotential height (gz500), and the geopotential thickness between 500 and 1000 hPa (gz500–1000). These are the most commonly used predictors in the statistical downscaling of precipitation (IPCC, 2007).

A procedure based on the forward selection stepwise regression technique and included testing with various linear and non-linear regression models was employed (Loukas et al., 2008). All of these models rely on homogeneous long time series of the target parameter on the local scale and one or several atmospheric predictors on the large scale. A major limitation is the assumption that the relationships obtained under present

conditions will also holdunder a changing climate. In this study, dummy variables (a set of twelve categorical variables assigned to the 12 months of the year) are used to account for the effect of the "month" on precipitation. The best regression downscaling model containing monthly dummy variables is expressed as (Loukas et al., 2008):

$$PMLR = a1 \cdot b1 + a2 \cdot b2 + a3 \cdot b3 + \ldots + a12 \cdot b12 + a13 \cdot mslp + a14 \cdot swa + a15 \cdot gz500 + a16 \cdot gz(500 - 100) + c \quad \text{(Eq. 4c)}$$

where PMLRis the logarithmically transformed monthly precipitation, b1, b2, b3, … , b12 are the monthly weighing dummy variables, a1, a2, a3, … , a12 are regression coefficients, and c is the regression constant. Dummy variables, b1−b12, are assigned binary values, 0 or 1, depending on the month in which precipitation is referred. For example, if the month is October, then, b1 takes the value of 1 and all the other dummy variables, b2−b12, take the value of 0. Similarly, if the month is November, then, b1 takes the value of 0, b2 takes the value of 1 and all the other dummy variables, b3−b12, take the value of 0 and so on. However, the monthly downscaled precipitation (PMLR) values will always have a smaller variance than the local values (i.e. areal observed precipitation) (Von Storch, 1999). In many climate impact studies the variance of the downscaled time series should be the same as the variance of the observed values. To meet this requirement various methods have been proposed such as variance inflation (Karl et al., 1990; Huth, 1999), expanded downscaling (Burger, 1996), and randomization (Dehn and Duma, 1999). In this study, to preserve the variability of the observed series, the estimated precipitation was combined with the residual values of the regression. These can be viewed as a noise component, statistically independent of the large-scale climate. In the formula:

$$P = PMLR + Presidual \quad \text{(Eq. 4d)}$$

with P = observed monthly precipitation, PMLR = monthly precipitation explained by multiple linear regression and Presidual = residuals of MLR. If this operation is carried out on the estimated series of the regression fitting period (October 1960–September 1990), the result is the observed series. For the climate scenarios, PMLR is obtained by downscaling the GCM outputs while Presidual remains unchanged. In this way, the problem of limited correlation between predictor and predictand variables may be tackled. However, to estimate the uncertainty of the downscaling method stochastic timeseries modelling was applied for the treatment of the residuals.

Stochastic simulation of hydrologic time series such as precipitation is typically based on mathematical models. For this purpose, several stochastic models have been suggested in the literature (Salas, 1993; Hipel and McLeod, 1994). Using one type of model or another for a particular case at hand depends on several factors such as the physical and statistical characteristics of the process under consideration, data availability, the complexity of the system, and the overall purpose of the simulation study. Given the historical record, one would like the model to reproduce the historical statistics. This is

why a standard step in hydrologic simulation studies is to determine the historical statistics. Once a model has been selected, the next step is to estimate the model parameters, then to test whether the model represents reasonably well the process under consideration, and finally to carry out the needed simulation study. The development of the stochastic model for Presidual was done again for the development period (1960–1990). Univariate stationary ARMA have been applied in the standardized monthly residuals. However, this procedure failed to reproduce the monthly residual correlations and periodic ARMA models have been fitted. The best-fitted model, according to the Akaike Information Criterion (AIC), was the Periodic Autoregressive Model of order four (4), PAR(4) defined as:

$$Presv,t \;=\; \phi 1,t\; Presv,t-1 \;+\; \phi 2,t\; Presv,t-2 \;+\; \phi 3,t\; Presv,t-3 \;+\; \phi 4,t\; Presv,t-4 \;+\; ev,t \qquad \text{(Eq. 4e)}$$

where $P_{resv,t}$, represents the monthly precipitation residual for year v and month(season) t; it is normally distributed with mean zero and variance σ 2 t (Pres); ev,t is the normally distributed and uncorrelated noise which has mean zero and variance σ 2t(e); and $\phi_{1,t}$. . . . $\phi_{4,t}$ are the monthly autoregressive parameters. Several statistics were estimated to evaluate Eq. 4e in simulating residual monthly precipitation for development and validation periods and then Eq. 4e was applied stochastically to generate 100 time series of the Presidual. The calculated residual precipitation timeseries were added to the downscaled P_{MLR} to reproduce the observed monthly precipitation pattern that was used in drought estimation using a meteorological drought index the SPI. Finally, the developed MLR equation (Eq. 3) was used to downscale monthly GCM precipitation time series PMLR for the future periods 2020–2050, and 2070–2100, and then the precipitation residuals ($P_{residual}$) were added to P_{MLR} using Eq. 4d, assuming that the precipitation residual time seriestime series in the future have the same statistical characteristics of the historical period. Essentially, the residual precipitation timeseries for the future periods were the timeseries generated by Eq. 4e for the historical base period.

After processing the information using SDS, the Mann-Kendall trend analysis will be applied. In this way, future trends can be analysed.

3. Study area

3.1. Climatology

The region is characterized by its aridity. The climatic variability in the region is due to the influence of the northwesterly trade winds. Following this trajectory, the clouds lose their humidity after crossing the geographical features of the area, reaching the Sonoran Plain without water. The predominant climate types in the basin are dry and semi-dry, while the humid and temperate climate types are restricted to the higher parts of the mountain ranges.

To differentiate the climatology of the region, Wladimir Köppen's world classification of climate types, modified by Enriqueta García (1964), was used as it better reflects the climatic characteristics of the Mexican Republic. This classification is based on the data of temperature and total monthly and annual precipitation and considers the existence of five fundamental climatic groups:

A. Warm humid;
B. Dry;
C. Humid temperate;
D. Boreal cold, intense winters;
E. Very cold, polar or high-altitude climates.

The climate types that exist in the study area are: temperate (C), in the high and middle areas and dry (B), in the middle and lower part (Fig. 4). In detail the climatic types that are abundant are:

- Type C(E)(w2)(x') of the more humid semi-cold temperate (C) group has a summer rainfall regime, winter rainfall is greater than 10.2% and the average annual temperature ranges between 5 and 12°C. It covers 13 km^2 and is located on the northern border of the Los Ajos Mountain range at altitudes of 2,500 m.a.s.l., with a predominance of pine, pine-oak and oak-pine forest vegetation.
- The climate C(w2)(x') of the temperate (C) group is more humid, has a summer rainfall regime, the winter rainfall is greater than 10.2%, and the average annual temperature ranges between 12 and 18°C. This climate type has an area of 4.34 km^2 and is dispersed in the northern part, in the mountain ranges and valleys of the north, at altitudes ranging between 1,830 and 2,340 m.a.s.l.
- Type C(w1)(x') of the temperate (C) to temperate-medium humidity group, has a summer rainfall regime, winter rainfall is greater than 10.2% and the average annual temperature ranges between 12 and 18°C. This climate covers 173.33 km^2 and is dispersed in the central-northern part of the park, in the mountains and valleys of the north, at altitudes ranging between 1,570 and 2,330 m.a.s.l., with a predominance of oak, pine-oak and oak-pine forests.
- Climate C(w1) of the temperate (C) to temperate-medium humidity group, has a summer rainfall regime, winter rainfall ranges between 5 and 10.2% and the average annual temperature ranges between 12 and 18°C. This climate covers an area of 10.17 km^2 and is located in the central part of the Aconchi Mountain

range, at altitudes ranging between 1,600 and 2,050 m.a.s.l., with a predominance of oak forest vegetation.

- The climate C(w0)(x') of the temperate (C) to temperate less humid group, has a summer rainfall regime, winter rainfall is greater than 10.2% and the average annual temperature ranges between 12 and 18°C. This climate covers 926.66 km^2 and is located in the northern limit of the study area, in the northern mountain ranges and valleys, at altitudes ranging between 1,380 and 1,960 m.a.s.l., with a predominance of natural grassland, oak forest, and oak-pine forest.
- Type C(w0) of the temperate (C) to less humid temperate group has a summer rainfall regime, winter rainfall ranges between 5 and 10.2% and the mean annual temperature ranges between 12 and 18°C. This climate covers 219.46 km^2 and is found in the central-northern part, in the Aconchi and San Antonio mountain ranges, at altitudes between 1,230 and 1,780 m.a.s.l., with a predominance of oak forest vegetation.
- The BS1kw(x') climate of the dry (B) semi-dry group, its rainfall is in summer and winter rainfall is greater than 10.2%, the average annual temperature ranges between 12 and 18°C, it has an area of 678.84 km^2, it is located in the northern part of the Los Ajos and Buenos Aires Mountain ranges at altitudes of 1,760 m.a.s.l.; the predominant vegetation is oak forest and natural pastureland.
- The climate of BS1kw belongs to the semi-dry (B) group. It has a summer rainfall regime, winter rainfall ranges between 5 and 10.2% and the average annual temperature is between 12 and 18°C. It covers an area of 2,618.97 km^2 and is located in the Aconchi, San Antonio, Cucurpe, Buenos Aires and Los Ajos mountain ranges, at altitudes ranging between 1,100 and 1,600 m.a.s.l. The predominant vegetation is oak forest, mesquite forest, natural grassland, microphyll desert scrub, induced grassland and subtropical scrub.
- Type (A)C(w0) of the temperate (C) semi-warm less humid group, has a summer rainfall regime, winter rainfall ranges between 5 and 10.2%, and the average annual temperature is higher than 18°C. It covers 1.15 km^2 and is located in the central part, in the Mazatán mountain range at altitudes of 1,400 m.a.s.l., with a predominance of oak forest vegetation.
- The BS1hw type of the dry (B) semi-dry group, has a summer rainfall regime, winter rainfall ranges between 5 and 10.2% and the mean annual temperature is higher than 18°C. It covers an area of 5,937.09 km^2 and is located in the central-northern part, in the northern mountain ranges and valleys, at altitudes ranging between 660 and 1,200 m.a.s.l., dominated by microphyllous desert scrub, induced grassland, desert mesquite, sarcocaulescent scrub, mesquite forest, subtropical scrub and oak forest.
- The BS0hw climate of the Dry (B) dry group, has a summer rainfall regime, winter rainfall ranges between 5 and 10.2%, and the average annual temperature is higher than 18°C. This climate covers an area of 3,350.65 km^2 and is located in the central part, between the Sonoran mountain ranges and plains at altitudes between 500 and 900 m.a.s.l.; the vegetation is dominated by microphyll desert

scrub, desert mesquite, subtropical scrub, sarcocaulescent scrub, induced grassland and mesquite forest.

- The BS0(h')hw type of the dry (B) dry group, has a summer rainfall regime, winter rainfall ranges between 5 and 10.2%, and the mean annual temperature is higher than 22°C. This climate type covers an area of 4,962.71 km^2 and is found in the central part between the Sonoran mountain ranges and plains at altitudes between 400 and 900 m.a.s.l., with a predominance of desert mesquite, mesquite forest, sarcocaulescent scrub, microphyll desert and subtropical vegetation.
- The BS1(h')hw type of the Dry (B) semi-dry group, with a summer rainfall regime, winter rainfall ranges between 5 and 10.2%, and the average annual temperature is higher than 22°C. This climate has an extension of 16.26 km^2, and is abundant in the central part of the study area, in the El Pajarito mountain range, at altitudes of 850 m.a.s.l., with a predominance of desert mesquite vegetation.
- The BWhw climate of the dry (B) to very dry group, has a summer rainfall regime, the winter rainfall ranges between 5 and 10.2%, and the average annual temperature is higher than 18°C. This climate covers an area of 1,094.87 km2 and is found in the central part, in the Sonoran mountain ranges and plains, at altitudes between 500 and 800 m.a.s.l. The predominant vegetation is microphilous desert scrubland, desert mesquite and sarcocaulescent scrubland.
- The BW(h')hw climate of the dry (B) group is very dry, has a summer rainfall regime, winter rainfall ranges between 5 and 10.2%, and the average annual temperature is higher than 22°C. This climate is the most extensive within the study area covering an extent of 7,953.51 km^2. It is found in the central-southern part, in the Sonoran mountain ranges and plains, at altitudes between 0 and 540 m.a.s.l. The vegetation is dominated by microphilous desert scrub, desert mesquite, sarcocaulescent scrub, induced grassland, sarco-crasicaule scrub, xerophytic halophilous vegetation and crasicaule scrub.

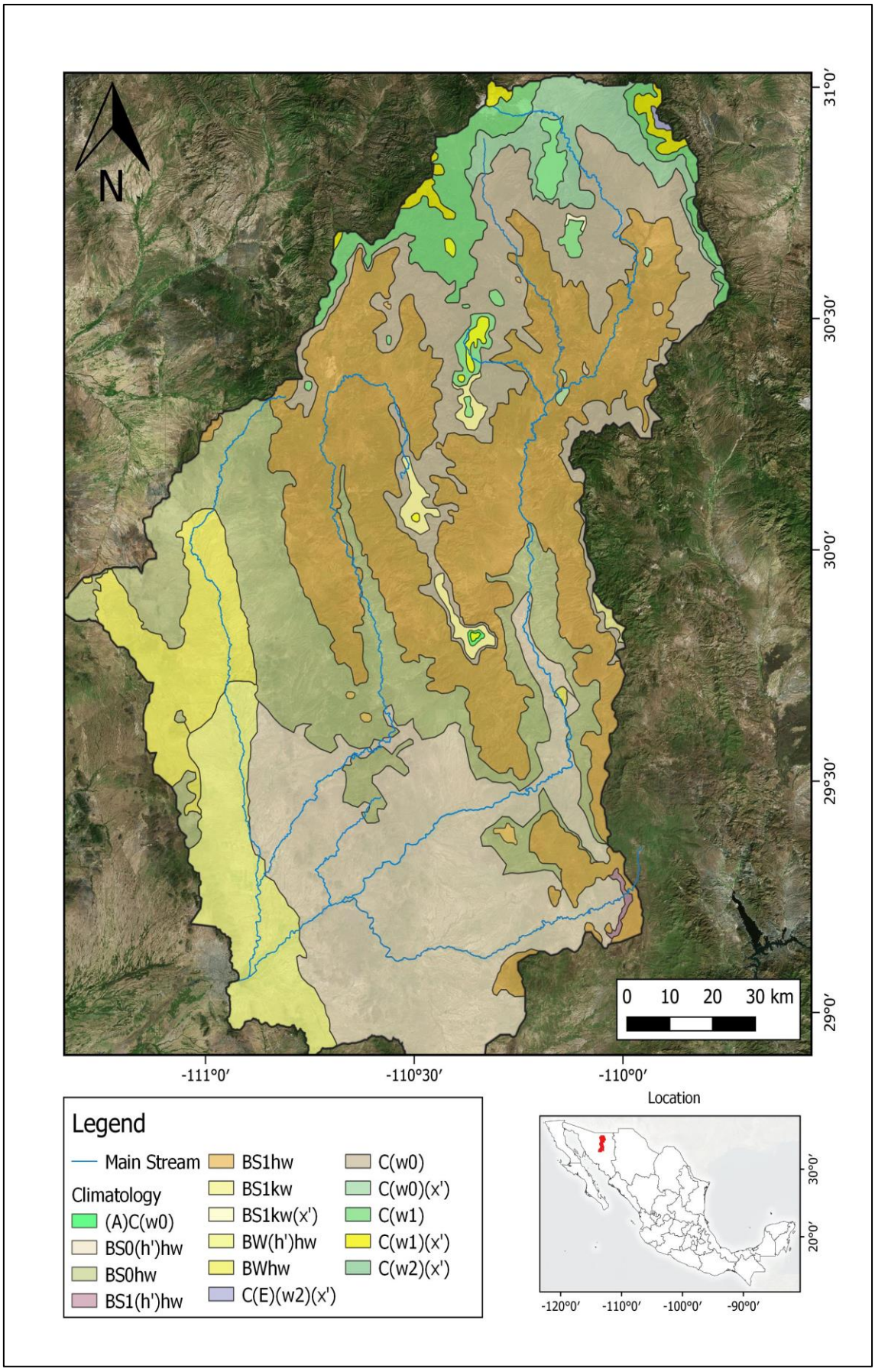

Figure 4. Difference in climatology of the region, River Sonora Basin.

3.1.1. Climatological stations

There are twenty-three operational climatological stations registered in the study area. The data covers the period from 1981 to 2015, with values of maximum, average and minimum temperatures, precipitation, number of days with rain, fog, hail and thunderstorms, as well as total evaporation. Although there are more stations downstream, they will not be taken into consideration because they are not relevant to the study carried out in this thesis.

In the upper part of the basin, where BVC is located, there are four climatological stations: Bacoachi, Bacanuchi, Arzipe and Cucurpe, which has the highest record of maximum temperature and total annual precipitation.

The stations are administered by the National Water Commission (CONAGUA) and monitored by the National Meteorological Service (SMN), the same agency that controls the defined variables and calculates precipitation and temperature averages and totals.

3.1.2. Precipitation

Precipitation has a defined pattern based on relief and altitude; the higher the elevation, the higher the precipitation; and the lower the altitude, the lower the precipitation.

Within the study area, the total annual precipitation ranges between 100 and 800 mm, from the northern limit to the northern part of the Rodolfo Félix Valdés Dam, the highest precipitation is between 500 and 800 mm. In the middle part, precipitation ranges between 300 and 500 mm, from the southern part of Sierra Cucurpe to the northern part of Sierra Libre. In the lower part, less precipitation occurs from the city of Hermosillo to the coastal limit, with total annual precipitation fluctuating between 100 and 300 mm (Table 2).

Table 2. Meteorological stations belonging to the Sonora River Basin that were used in the analysis.

Station	Code	Municipality	Coordinates		Altitude (m.a.s.l.)	Precipitation (mm/year)
			Longitude (W)	Latitude (N)		
Arzipe	26005	Arzipe	110°16'80''	30°33'60''	836	474.3
Bacanuchi	26007	Arzipe	110°23'90''	30°59'90''	1049	511.1
Bacoachi	26145	Bacoachi	109°97'00''	30°63'20''	1049	514.4
Cucurpe	26025	Curcupe	110°70'60''	30°33'10''	853	579.9

3.2. Geology

The lithology of the Sonora River Basin consists of:

Precambrian PE (E): The outcrops of this era are located in the north-eastern part of Sierra Los Ajos and east of the City of Cananea. These rocks represent 0.02% of the total area and are important because they are the oldest rocks in the country and form the stratigraphic basement of the study area. The Precambrian outcrops consist of metamorphic rocks, mainly schist, which are complemented by gneiss.

Palaeozoic. Palaeozoic rocks are distributed mainly in the central part of the Sonora River basin, in the north-eastern and central-eastern portion of the study area. The lithology is dominated by limestones (1.77%) and in smaller proportion by granite, sandstone and metamorphic complex (quartzite).

- Limestone P (cz), and sandstone P (ar): These together cover 1.94%, within the same sedimentary rocks that characterise the Palaeozoic, mainly limestone which occurs in a dispersed manner in the central part of the basin east of the city of Hermosillo and south of San Miguel de Horcasitas. Due to the dispersed nature of these outcrops and the arrangement of the occurrences, it is not possible to establish with certainty their full stratigraphic correlation. The sandstone ranges from orthoquartzite to sub-grauwacke, and is exposed south of the town of Rayón, sometimes interspersed with shale and conglomerate horizons. The sandstone outcrops have a smooth morphology in a tended lomério. The limestone, like the sandstone, is considered a shallow platform-type environment, the limestone varies in structure; from calcilutite to oolitic type, in some places, there are laminar and thin horizons of flint and shale. Near the city of Hermosillo, carbonate rocks are exploited for lime, cement and marble production. The intrusive magmatic events of the Tertiary transformed the limestone into marble.
- P(Gr) granite: Palaeozoic intrusive outcrops cover 0.05% of the area, with outcrops south of the Los Ajos Mountain range and the southern portion of the Buenos Aires Mountain range. They consist of biotite granites of phaneritic texture, affected by pegmatitic dykes and intrusions of more recent mainly Cretaceous rocks, the granite ex positions present soft morphology and in some places "onion" type weathering.

Mesozoic: The variety of rocks of this era has historical and tectonic relevance in northwestern Mexico. In the study area, these rocks occupy 17.22% of the extent, those of intrusive origin characterise it and are complemented by sedimentary, volcanic and metamorphic materials.

- Lutites and sandstones TR-J (lu-ar): These rocks are located north of the locality La Colorada, in a strip oriented north-south. They belong to the Barranca Formation deposited in a transitional environment. The sequence is completed with anthracite and graphite horizons when metamorphism is present; horizons and lenticular structures of siltstone, flint and conglomerate are also present in

several portions of the sequence. Moreover, it presents carbonate material probably from a lagoon environment.

- Limolite-sandstone-conglomerate J (lm-ar-cg), and siltstone-sandstone Js (lu-ar): The rocks of these systems in the study area are of sedimentary type and are presented in two lithological sequences, one formed by siltstone, sandstone and conglomerate; the other by siltstone and sandstone. In general, they are formed in a shallow marine environment; both sequences are complemented to a greater or lesser extent by shale, silty sandstone, calcareous, mudstone, orthoquartzite and conglomerate horizons. Their distinctive feature is the dark reddish and greenish colouration of the siltstone. Representative outcrops are found in the surroundings of the town of Cucurpe.

Cretaceous: Intrusive rocks are dominant and complemented by sedimentary and volcanic rocks.

- Diorite-granite-granodiorite K (D-Gr-Gd): The intrusive outcrops are formed mostly by granite and to a lesser extent by granodiorite and diorite, the textures are coarse and coarse, and the granitic massifs have several intrusions of pegmatitic and lamprophyric dykes, which extend for kilometres. The plutonic materials are present in the Aconchi and El Pajarito mountain ranges, as well as in the Sierra de Aconchi and El Pajarito mountain ranges located north of the city of Hermosillo. In proportion, these rocks occupy 10.97% of the study area.
- Limestone-limolite Ki (cz-lm), Limestone-limolite-sandstone-conglomerate, K (lu-lm-ar-cg), sandstone-acid tombstone Ks (ar-ta): Sedimentary rocks are distributed in three locations, 20 km south of the town of Cucurpe, another in the San Antonio mountain range and one more northeast of the town of San Miguel de Horcasitas. Three units can be differentiated in the sedimentary rocks: the first is formed by shale, siltstone, sandstone and conglomerate, the second by limestone and siltstone and the third by sandstone-acid tuff. The three groups are formed in a shallow platform environment with volcano-sedimentary influence.
- Andesite K(A), and acid tuff K(Ta): Volcanic rocks are scarce in the Cretaceous, they are limited to andesites and acid tuffs, cropping out south and northeast of the towns of Bacoachi and San Miguel de Horcasitas, respectively.
- Granite M (Gr), gneiss M (Gn) and conglomerate M (cg): These rocks of Mesozoic age do not have a defined period or stratigraphic level, occupying less than 1% of the study area. These rocks are mainly granites, conglomerates and regional metamorphic rocks such as gneiss, their outcrops are found north of the Sierra Mazatán on the western flank of El Bamuco Creek.
- Soils (Q): Outcrops belonging to the Cenozoic and occupy 80.76% of the study area while soils are representative with 34.5%. There are mainly alluvial soils complemented by aeolian, littoral and marshy deposits. The soils define the

landscape of the lower middle part of the study area, especially the agricultural valley of Costa de Hermosillo.

- Sandstone-limolite-conglomerate-lutite T (ar-lm-cg-lu): The rock unit formed by sandstone, siltstone, with glomerate and shale, is a fundamental part of the continental clastic fills of the gravity tectonic trenches located along the Sonora, San Miguel de Horcasitas and Zanjón rivers covering an extent of 22.28%.
- Rhyolite-acid tuff TOM(R-Ta): The acid rhyolite-acid rhyolite-toba volcanic sequence of the middle Tertiary belongs to the sequences that form the Sierra Madre Occidental, it also contains intercalations of conglomerate, sandstone and vitrophyres. These volcanic rocks dominate the northern part of the study area in the San Antonio mountain structure and the mountain ranges to the southeast of the Heroica Ciudad de Cananea, constituting 17.23% of the study area.
- The Cenozoic also includes other lithologies, mainly volcanic rocks of intermediate composition such as basalt that outcrops in the surroundings of the town of Banámichi; sandstones, conglomerates, granites, volcanic breccias and metamorphic rocks such as cataclasite. Their outcrops are scattered across the study area.

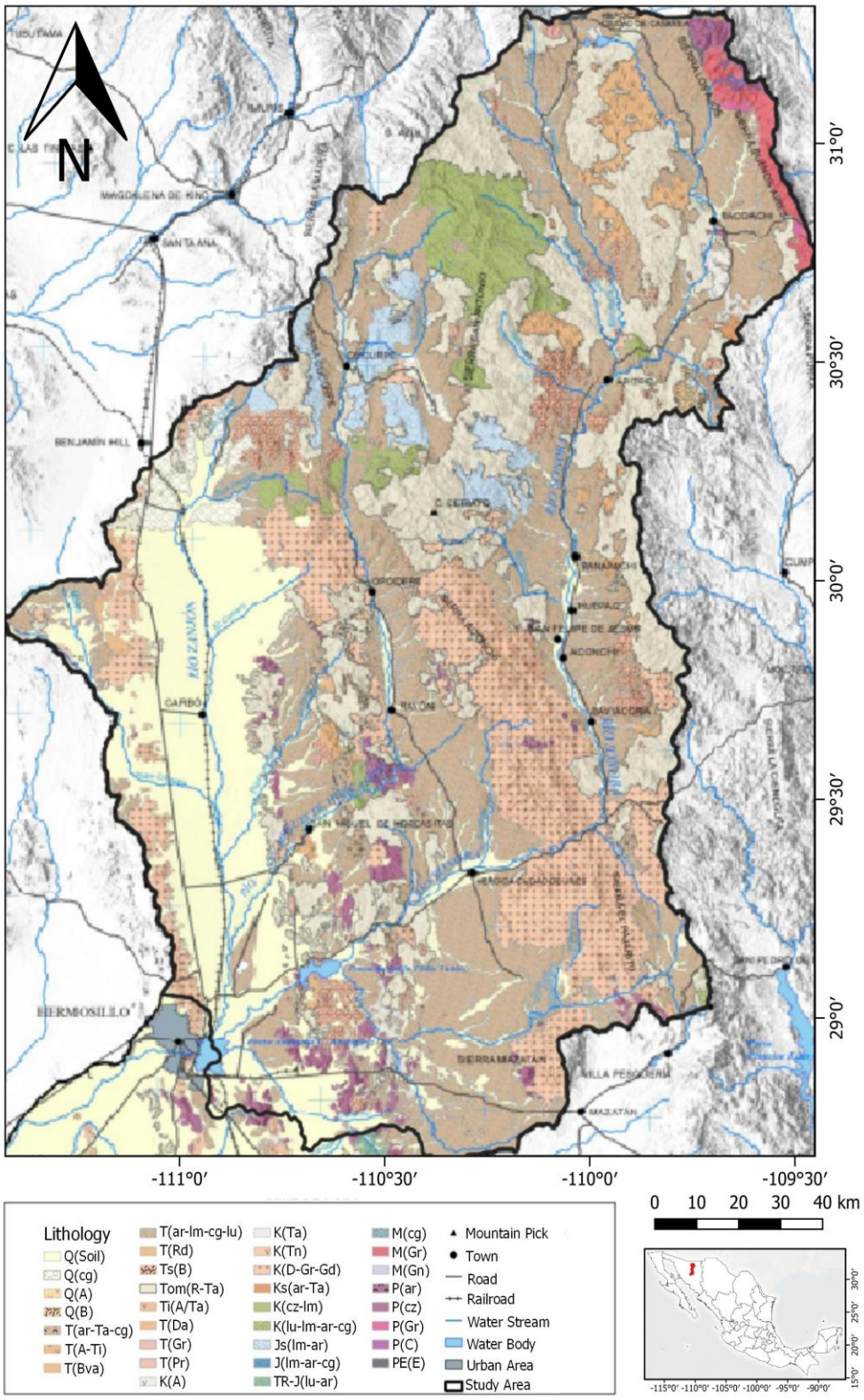

Figure 5. Geological map of the Sonora River Basin. Modified from INEGI (2017).

In general, the main morphological forms present in the study area are mainly valleys, mountain ranges and terraces. The study area is geomorphologically characterised by the presence of a series of parallel mountain ranges and hills, with a northeast-southeast orientation and separated by narrow valleys. The valleys are constituted by Tertiary and Quaternary deposits; the mountain ranges by intrusive, sedimentary, volcanic and metamorphic rocks and the terraces by conglomerates of the Báucarit Formation (King, 1939).

The Sonora River sub-basin is the most developed, since it occupies an area of about 1,500 km2; it has its natural limit in the northern foothills of the Sierra Madre Occidental, starting the development of the river in the vicinity of the city of Cananea at a point called Ojo de Agua de Arballo, joining downstream numerous streams formed in the eastern flank of the Sierra del Manzanal and those of the western flank of the Sierra de los Ajos. It rises at an altitude of 1,970 m.a.s.l., following a north-south course to the town of Mazocahui; from there to its confluence with the San Miguel River the riverbed has carved the valleys of Ures and Topahue, cutting through three narrows of intrusive and metamorphic rocks, draining with a rectangular type of drainage, due to the structural control of the area.

In the study area, the rocks are of Precambrian to Quaternary age. Throughout its extension, it includes lithology of igneous, metamorphic and sedimentary origin (Fig. 5).

Part of the morphology present in the area is the result of early Cenozoic volcanism, which culminated in an extensional tectonic event that generated erosional and continental depositional processes known in northwestern Mexico as the Basin and Range geological province.

3.3. Hydrology

Sonora River has eleven sub-basins. In the current study, only the following six shall be considered (Fig. 6). These are the Sonora River itself, the Bacanuchi River, the Banamichi River, the La Junta Stream, the El Zanjon River and the San Miguel River (Table 3).

- Sonora River Sub-basin: It is located in the north-eastern end where the Sonora River stems from. The main channel originates from run-off from the Cananea, Los Ajos and Manzanal mountain ranges, which is locally called the Bacoachi River. It has a catchment area of 6,828,864 km2 with an altitudinal range of 839 to 2,109 m.a.s.l.
- Bacanuchi River Sup-basin: Its main source is homonymous with the river, born with the name of Los Alisos Stream, which changes its name to Las Bellotas Stream before the town of Bacanuchi, it is properly the Bacanuchi River. In the final part of the sub-basin the run-off from the Piedra de Lumbre Stream is received, upstream from the town of Arizpe, this hydrography joins the Sonora River. The altitude of the sub-basin ranges from 859 to 2,260 m.a.s.l. and a catchment area of 1,615,770 km2.
- Sonora-Banamichi River Sub-basin:. It is located in the middle part towards the eastern end, has a catchment area of 6,828,864 km^2, its altitudinal range is from 286 to 1,776 m.a.s.l.; on the left bank, the waters of the La Junta Stream sub-

basin are incorporated at the Rodolfo Félix Valdés Dam, this has a catchment area of 2,064,920 km2 with an altitudinal range of 285 to 1,610 m.a.s.l.

- San Miguel River Sub-basin: This is flanked by the Zanjón River Sub-basin to the west and the Sonora-Banamichi River to the east, with an area of 4,187,750 km^2 and an altitudinal range of 247 to 2,203 m.a.s.l., its main channel is the San Miguel de Horcasitas River, which receives contributions from the Sarachi, El Tanque and El Bajío streams on the left bank. At the end of the sub-basin, it is joined on the right bank by the El Zanjón River, which is the main hydrography of the sub-basin of the same name. The San Miguel River ends at the Abelardo L. Rodriguez Dam where it joins the Sonora River.
- Zanjón River Sub-basin: Its main source is the river of the same name, with a catchment area of 5,710,381 km^2 and an altitudinal range from 327 to 1,609 m.a.s.l., The hydrography begins with the name Otates Stream which changes downstream as Purgatorio at the height of the connection on the left bank with the El Chi stream not upstream of the town of Qurobabi is when it is properly the Zanjón River, continuing and on the right bank it receives the El Chinoso and Pozo Crisanto streams, and on the left bank the contribution of the Punta de Agua stream. The Zanjón River ends when it intersects the San Miguel River in the sub-basin of the same name.
- La Junta Stream Sub-basin: It is located south of the Sonora-Banamichi River sub-basin, with an area of 2,054,900 km^2 and an altitudinal range of 285 to 1,441 m.a.s.l. The sub-basin is characterised by being formed by two main streams: the Grande Stream in the centre east and the Noria Colorada Stream in the centre south, both of which flow into the San Francisco Stream that flows into the Rodolfo Félix Valdés Dam.

Table 3. Area and mainstream length of the Sonora River sub-basins.

Sub-basins name	Area (km^2) (	Main Stream Lenght (km)
Sonora River	6,828,864	272.86
Bacanuchi River	1,615,770	83.45
Banamichi River	2,064,920	130.56
El Zanjon River	5,710,381	153.22
San Miguel River	4,187,750	254.66
La Junta Stream	2,054,900	121.54

3.4. Hydrogeology

Located in a semi-desert region and having very limited surface water, which can satisfy the vital needs of the population and the demands of this resource by the Irrigation District in the Hermosillo Coast. The ground water constitute the most important source of water supply.

The agricultural zone of Hermosillo began to develop in 1947 with 17 wells, which were integrated to constitute Irrigation District No. 51, which was created in 1948, and 1953 was named: Costa de Hermosillo. The number of uses over time has undergone a strong increase; thus, by 1955 there were already 474 wells. By 1999, the volume of extraction was already being carried out by 498 wells, being of the order of 400 Mm^3/year, of which 393 Mm^3 were used for agricultural use, 5 Mm^3 for public use and 2 Mm^3 for domestic use.

The Sonora River aquifer is contained in a porous and permeable medium made up of unconsolidated boulders, gravels, and sands, restricted to the riverbeds and tributary streams, they present good granular porosity and therefore are sediments regularly of good permeability and even more so when they present good classification. These sediments currently constitute the local aquifer. It is of the free type whose lateral boundaries correspond to intrusive igneous rocks of the granitic type and extrusive rocks of the rhyolitic and andesitic type. In some areas, such as the valleys of Ures and San Felipe de Jesús, where the aquifer has its greatest amplitude dimensions, the Baucarit formation outcrops out, which is a conglomeratic complex aquifer system of medium to low permeability.

The depth of the impermeable basement varies from about 15 m in the narrows of the riverbed to about 200 m where it is more extensive. In the Sonora River sub-basin, transmissivities vary between $1x10^{-3}$ and $84x10^{-3}$ m^2/s. Exploitation of the aquifer has not significantly modified the natural pattern of groundwater flow.

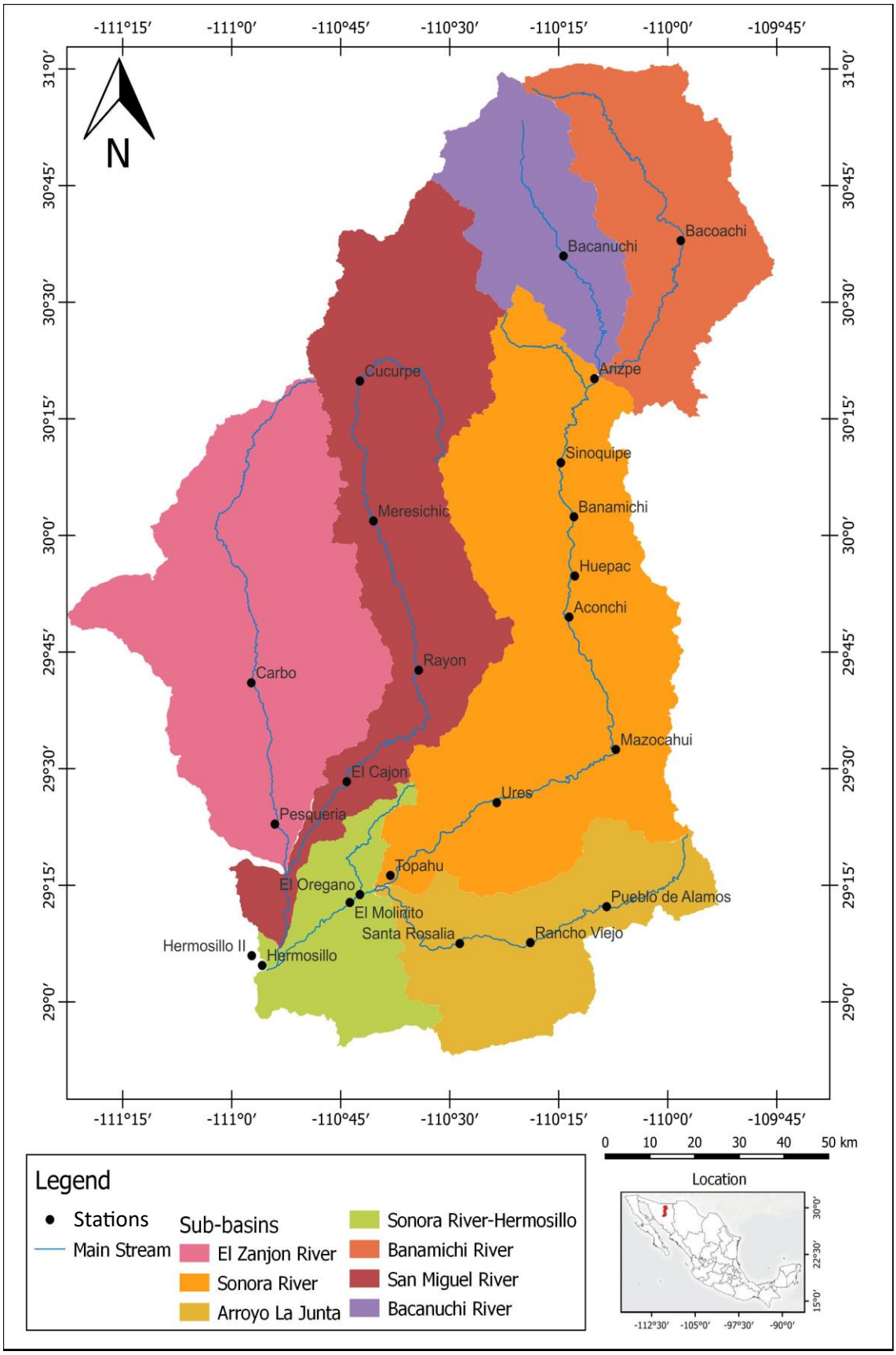

Figure 6. Sonora River sub-basins considered in the current study and their main streams.

4. Results

This chapter describes the results obtained after applying the methodology that has been described in previous chapters.

4.1. Checking data homogeneity

To use satellite data from CHIRPS for the processing of climate series, homogeneity has been analysed by the double mass curve analysis. In this case, the comparison has been carried out between the data from the Bacanuchi meteorological station and its equivalent CHIRPS data (Fig. 7). In order to make this comparison, data equivalent to the period 1981-2015 was used. This time period is the one for which the meteorological stations have records. Therefore, if we want to use the CHIRPS climate series, which is more complete, we will apply this methodology.

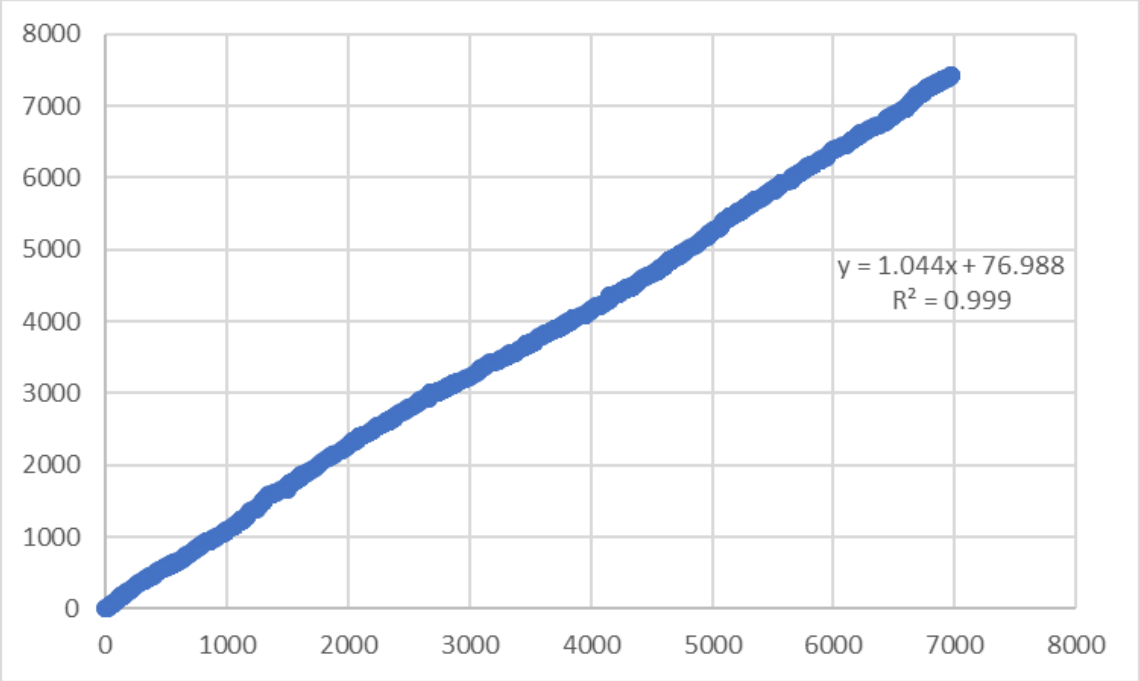

Figure 7. Graphical representation of the dual mass analysis between the Bacanuchi meteorological station and the satellite equivalent data (CHIRPS). The axes show the cumulative daily precipitation for the period 1981-2015.

For this thesis, the data corresponding to Bacanuchi will be used, because it is the closest station to the mine, so it's rainfall data will be the most similar to those of Bordo Poniente. Before correlating the weather stations data and the satellite data, it is necessary to determine if the station values are representative of the region. For this purpose, the double mass method has been applied to the six stations closest to Bacanuchi (Fig. 8). These are Arzipe, Bacoachi, Banamichi, Curcupe, Meresichic and Sinoquipe.

Applying the double mass method, it is observed that the homogeneity of the climate station and satellite data is good enough to work with the data obtained from the CHIRPS database. Furthermore, when checking the homogeneity of the Bacanuchi data with respect to the nearest stations, it is good. Therefore, we can say that it is a representative climatic series for the study region.

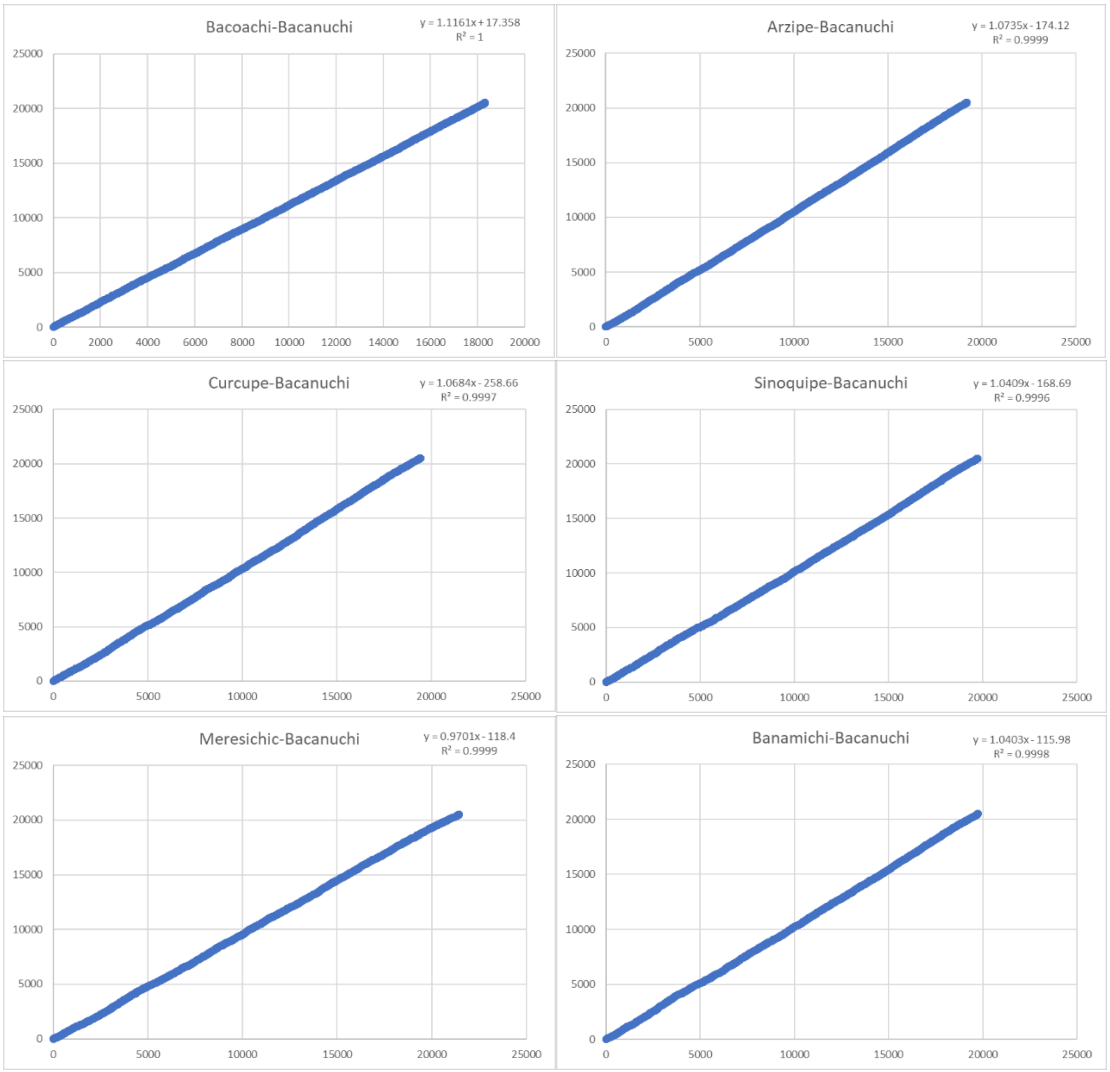

Figure 8. Graphs representing the double mass curve analysis, in which the data from Bacanuchi are compared with those from the 6 stations closest to it. The axes show the cumulative daily precipitation for the period 1981-2015.

4.2. Frequency analysis and probability plotting

This section shows the results corresponding to the frequency analysis and probability plotting, using the RAINBOW software.

4.2.1. Estimation of the probability of exceedance

To estimate the probability of exceedance, the Weibull (1939) method was used. In this case, the annual precipitation values for the years 1981-2022, obtained from CHIRPS, were used, which were processed using the RAINBOW software, resulting in Table 4.

Table 4. Probabilities of exceedance of the ranked annual rainfall estimated with Weibull method.

Ranked rainfall X (mm)	Rank number r	Estimate of the probability of exceedance Px, Weibull (%)
692	1	0.89
658	2	2.45
623	3	5.70
622	4	5.75
592	5	11.27
590	6	11.72
589	7	11.82
570	8	16.20
566	9	17.87
562	10	19.19
553	11	22.00
550	12	22.88
545	13	24.70
532	14	29.76
519	15	35.00
514	16	37.42
499	17	43.93
499	18	44.20
489	19	48.50
480	20	52.66
479	21	53.29
472	22	56.25
462	23	60.66
457	24	63.00
455	25	63.66
454	26	64.50
446	27	67.50
432	28	73.00
428	29	74.50
424	30	76.00
418	31	78.00
416	32	79.00
416	33	79.00
411	34	82.50
411	35	86.00
403	36	86.00

391	37	93.00
391	38	93.00
362	39	95.00
358	40	95.00
339	41	96.00
337	42	96.00

4.2.2. Probability plot

A probability plot i.e., comparing rainfall intensity versus exceedance probability, allows for a graphically checking of the distribution assumptions. (Fig. 9). When the data are plotted on arithmetic paper, where both axes have a linear scale, the data are not likely to be on a straight line but to follow an S-shaped curve. This plot is sometimes called a percentage ogive.

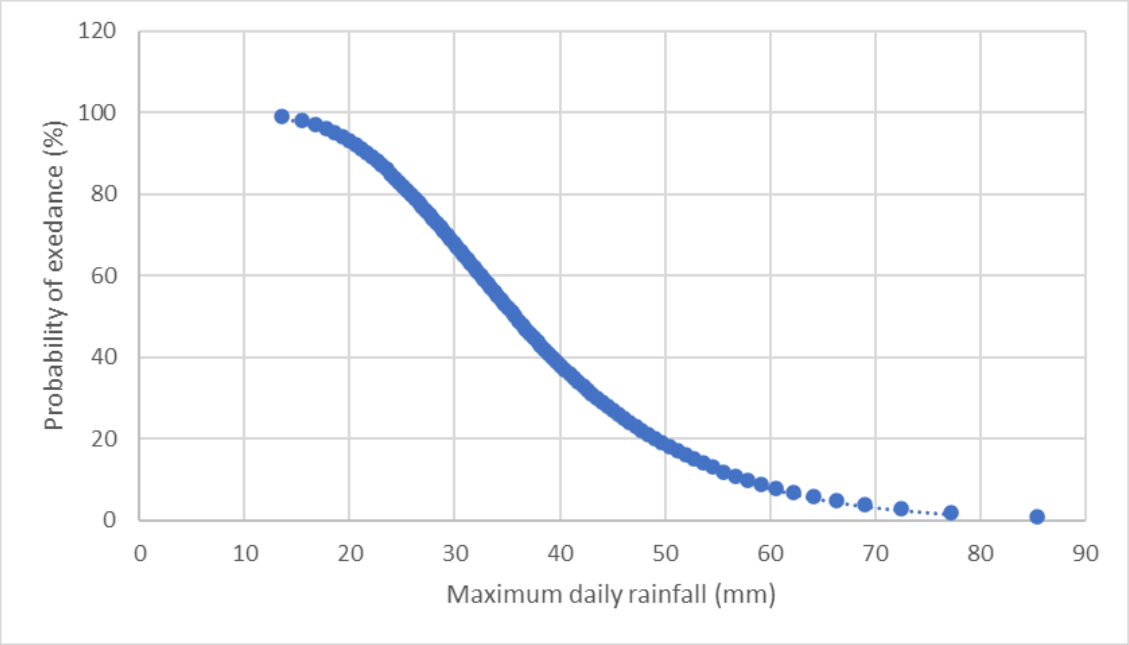

Figure 9. Probability plot of the total annual rainfall for Bacanuchi station by using linear scales for both axes.

The distribution shown in Figure 9 shows that the climate data follows a uniform distribution. It can be seen that most of the annual rainfall values are close to the average, while extreme values are rare. Therefore, the number of years with high rainfall that could pose a risk to the Bordo Poniente dam is very small.

4.2.3. Estimating rainfall amounts for selected probabilities

This methodology can be applied using either graphical or numerical methods. In this case, numerical methods were followed (Table 5) and the return period was obtained.

Table 5. Estimated annual rainfall for Sonora Basin for selected probabilities and return periods derived from the fitted line in the probability plot.

Probability of exceedance Px (%)	Estimated annual rainfall (mm)		Return Period Tx (years)
	$\bar{X}$ + k s $\bar{X}$ – k s	Xp	
10	486.336 + 1.28 (87.16) =	597.901	10.00
20	486.336 + 0.84 (87.16) =	559.551	5.00
30	486.336 + 0.53 (87.16) =	532.531	3.33
40	486.336 + 0.255 (87.16) =	508.562	2.50
50	486.336 + 0 (87.16) =	486.336	2.00
60	486.336 - 0.255 (87.16) =	464.111	1.67
70	486.336 - 0.53 (87.16) =	440.142	1.43
80	486.336 - 0.84 (87.16) =	413.122	1.25
90	486.336 - 1.28 (87.16) =	374.772	1.11

4.2.4. Estimates of extreme rainfall (Gumbel distribution)

To determine the return period of extreme rainfall, the Gumbel methodology was followed. The result is a table (Table 6), in which the recurrence period associated with a certain amount of mm/day is reflected. It can be seen that the most important precipitations, those that can pose a risk to mining installations, have a return period of more than a thousand years. This means less risk to the infrastructure.

Table 6. Annual daily maximum rainfall (mm) and its associated payback period (years).

Annual daily maximum rainfall (mm)	Return period (years)
10	0.9
20	1.0
30	1.1
40	1.5
50	2.3
60	3.8
70	6.7
80	12.2
90	22.6
100	42.3
110	79.6
120	150.1
130	283.5
140	536.0
150	1,013.7
160	1,917.6
170	3,627.8
180	6,863.7
190	12,986.5
200	24,571.4

4.2.5. Intensity-Frequency-Duration Analysis (IDF)

As 42 years of uninterrupted daily data were available, it was possible to produce the IDF curves (Fig. 10). These consist of the graphical representation of the maximum annual rainfall for the periods of 1, 2, 3, 4 and 5 days concerning the return periods for these same periods (Table 7).

Table 7. Mean maximum rainfall (mm) for the periods of 1, 2, 3, 3, 4 and 5 days, with their associated return periods.

Duration	Return Period T (years)						
	2	5	10	25	50	100	250
1 day	37.81	49.08	54.98	61.27	65.33	68.98	73.34
2 days	24.19	31.54	35.38	39.48	42.12	44.50	47.34
3 days	18.76	24.13	26.94	29.94	31.88	33.62	35.70
4 days	15.12	19.09	21.16	23.38	24.81	26.09	27.63
5 days	13.03	16.40	18.17	20.05	21.27	22.36	23.67

The results in Figure 10 show the different return periods for rainfall over a period of one to five days. In the case of the most extreme rainfall, these hardly exceed 70 mm in one day for a return period of 250 years. Rainfall that could cause damage to infrastructure would therefore have to have a longer return period. This poses a lower risk to Bordo Poniente.

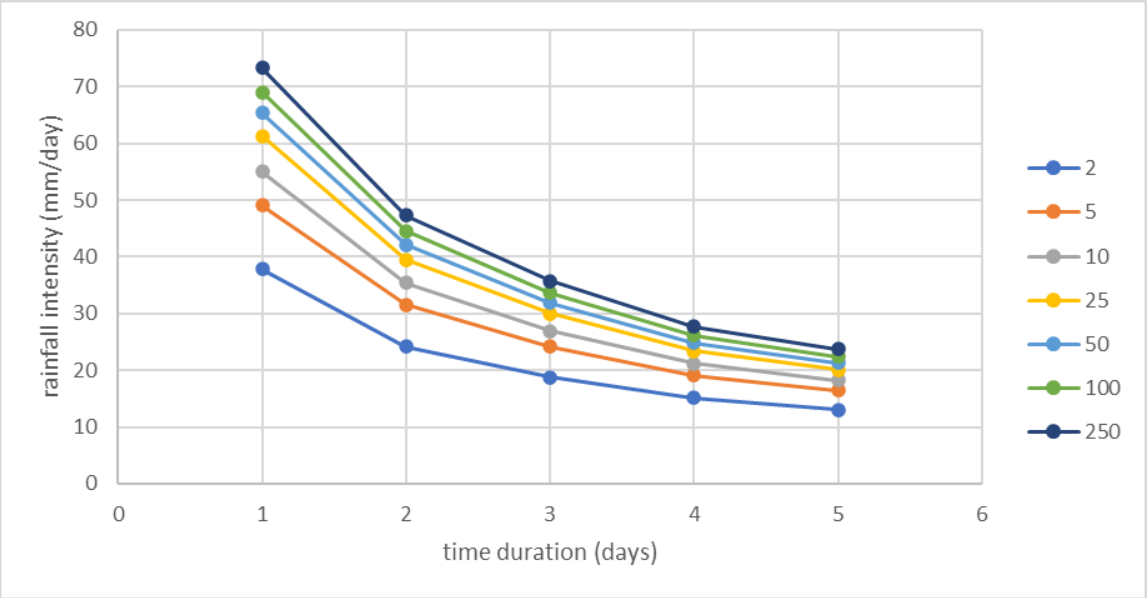

Figure 10. Representation of the IDF curves for the Bacanuchi station data. The different lines indicate the return period, in years ,for that precipitation to occur.

4.3. Pre-Spillage Precipitation Analysis

For this section, rainfall that could have affected the mine's infrastructure before the spillage event was taken into consideration. In this case, the only rainfall with sufficient capacity to be considered is the one that occurred on 8 and 9 July 2014, which consists of an accumulated rainfall of 87.2 mm.

In this case, five different scenarios were considered according to the runoff area (Fig. 11). All except scenario 5 consider areas exclusively upstream of Bordo Poniente so that all the water will affect the dam. In the case of Scenario 5, the retention produced by the containment bund will be deducted, which is equivalent to 2,370 m^3 of acid solution. To all the scenarios, 40,000 m^3 of acid solution stored in Bordo Poniente will be added and 150 m^3/h will be deducted based on the pumping capacity of the dam.

At BVC Copper is obtained by irrigating piles of copper-rich material with water of pH 1.4. By considering that all of the irrigated water reaches the Bordo Poniente or in the case of scenario 5 the Nuevo Bordo, shall be considered that the precipitation will reach its destination in its entirety without being affected by infiltration. In cases 1 and 2, only the surface area corresponding to the piles of copper-bearing material is considered, as it is considered to be prepared to lose as little of this acid solution as possible. For cases 3 and 4, half and the whole area of the drainage basin of Bordo Poniente were considered, respectively. In this case, it is considered that as this is an area of volcanic material, in which infiltration occurs through fractures, these will not play an important role in the company's desire to collect water for use in mining. Therefore, infiltration will be negligible. The last and largest case is scenario 5, which considers the capacity of the new board to cope with extreme rainfall.

The first scenario considers only recent and therefore active irrigation piles. The second scenario considers the entire area where this practice has been carried out. The third scenario not only considers scenario two, but also includes the area corresponding to the Bordo Poniente drainage network south of the second scenario. Scenario four considers the entire drainage basin towards Bordo Poniente (Fig. 11).

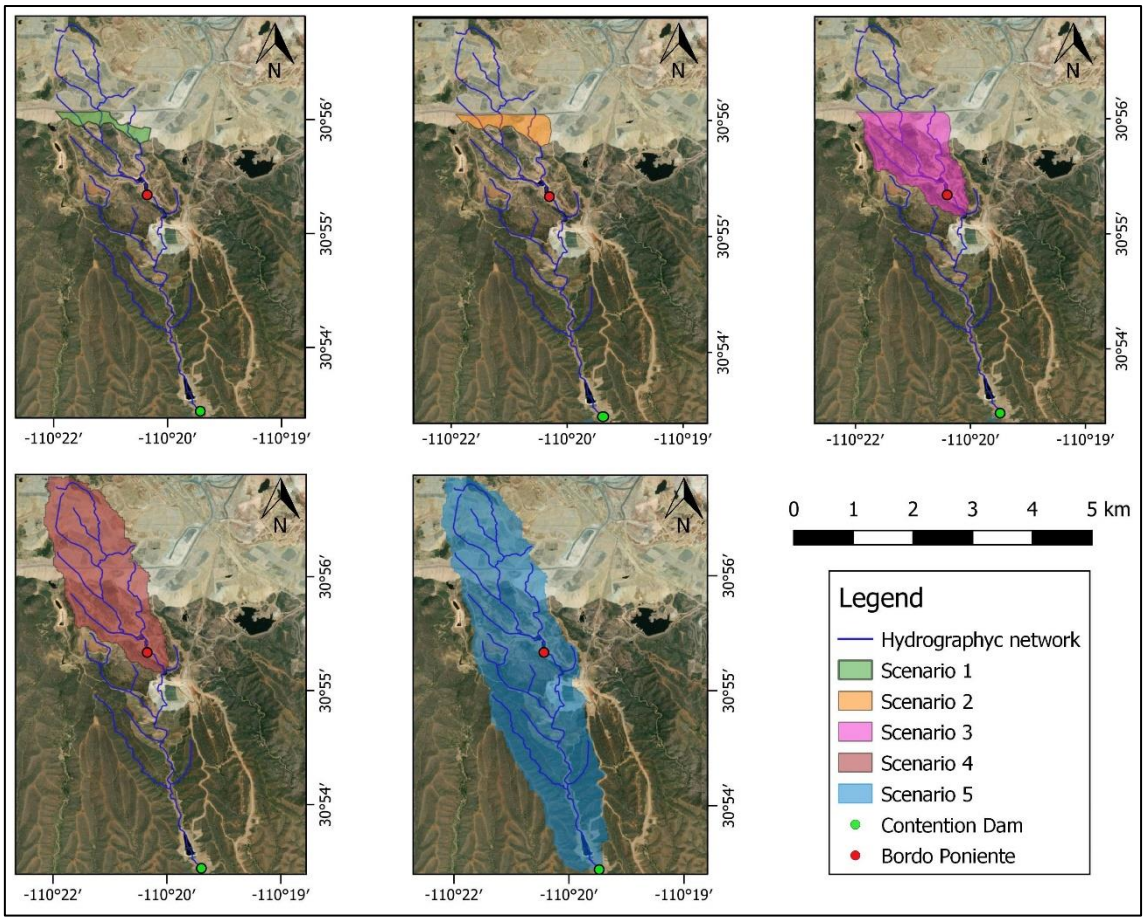

Figure 11. Representation of the five scenarios considered in pre-spillage precipitation analysis.

When obtaining copper by irrigation, all the water that infiltrates will be considered to finally reach Bordo Poniente.

In the study area, evapotranspiration is 88%, so we will deduct this percentage from the climatic series. The water that will end up in Bordo Poniente is 10% infiltration and 2% runoff, as we will consider that the area is prepared to capture all the water possible without losses,. In the first case we will discount it to simulate the case in which losses occur in the system. In the second case we will consider that this runoff ends up completely in Bordo Poniente. Therefore, two scenarios will be considered, with 10 and 12% infiltration. In the case of the 12% scenario, 2% surface runoff is added to the total water reaching the dam. For both cases, the 40,000m^3, which is equivalent to one-third of the dam's capacity, is usually stored in the dam for use in copper production.

As can be seen in Tables 8 and 9, none of the scenarios exceeds the amount of precipitation that would pose a danger to the integrity of Bordo Poniente, as it does not exceed (in cases 1 to 4) the amount of 120,000 m^3. In the fifth scenario, 800,000 m^3 should be exceeded, because this is the capacity of the dam built downstream.

Table 8. Representation of the results of scenarios 1 to 5 for 10% infiltration. To this amount, have been added to the 40,000m^3 already in Bordo Poniente.

Hours of rainfall	Scenario 1 (m3)	Scenario 2 (m3)	Scenario 3 (m3)	Scenario 4 (m3)	Scenario 5 (m3)
2	42,853	43,721	58,652	75,714	120,818
6	42,253	43,121	58,052	75,114	120,218
10	41,653	42,521	57,452	74,514	119,618
16	40,753	41,621	56,552	73,614	118,718
24	39,553	40,421	55,352	72,414	117,518
32	38,353	39,221	54,152	71,214	116,318
40	37,153	38,021	52,952	70,014	115,118
48	35,953	36,821	51,752	68,814	113,918

Table 9. Representation of the results of scenarios 1 to 5 for 12% infiltration. To this amount, have been added to the 40,000m^3 already in Bordo Poniente.

Hours of rainfall	Scenario 1 (m3)	Scenario 2 (m3)	Scenario 3 (m3)	Scenario 4 (m3)	Scenario 5 (m3)
2	43,484	44,525	62,443	82,917	137,042
6	42,884	43,925	61,843	82,317	120,218
10	42,284	43,325	61,243	81,717	119,618
16	41,384	42,425	60,343	80,817	118,718
24	40,184	41,225	59,143	79,617	117,518
32	38,984	40,025	57,943	78,417	116,318
40	37,784	38,825	56,743	77,217	115,118
48	36,584	37,625	55,543	76,017	113,918

4.4. Trend analysis

This chapter shows the results of analysing the trend of annual and seasonal extreme events by the Mann-Kendall method, by using the climate data series equivalent to the period 1981-2022 (Annex I). Among the data obtained in this analysis, one of the most interesting for determining the trend is Sen's slope (S). A positive S value means that the trend is increasing, and a negative S value means that the trend is decreasing. This will be taken into account to determine the trends. If the p-value of the test is lower than some significance level (common choices are 0.10, 0.05, and 0.01), then there is statistically significant evidence that a trend is present in the time series data. So when these are below 0.1, the trends are considered to be significant.

In the first case, the number of extreme events was analysed, produced for rainfall in periods of 1 to 5 days (Table 10). In this case, a clear negative trend is observed, except for two cases where a slight increase is seen, but it is too small to be relevant. This would indicate that the number of events would be reduced.

Table 10. Sen's slope (S) for the different extreme rainfall events.

Time period (days)	> 20mm	> 30mm	> 40mm	> 50mm
1 day	-177	46	-15	10
2 days	-122	-143	-28	-28
3 days	-72	-125	-60	-35
4 days	-80	-109	-42	-113
5 days	-80	-110	-52	-79

The second case analysed is that which corresponds to the trends in total rainfall by season and year (Table 11). In this case, a decrease in rainfall is observed in all seasons except for those occurring in summer. Summer is also the season with the highest rainfall, and this increase is much more important than the decreases that occur in the other cases.

Table 11. Sen's slope (S) for the different seasonal rainfall trends.

Spring	Summer	Autumn	Winter
-4	78	-178	-244

4.5. Global climate projection

In this section, the monthly precipitation data downloaded from Copernicus (2023) are analysed. In the first instance, the data were processed by the statistical downscaling method (SDS), to homogenise the climate series of the different experiments concerning the Bacanuchi data. Once the information had been processed, the trend was analysed using the Mann-Kendal method, as in previous sections.

In the first case, trends in monthly rainfall were analysed. To determine the trend, the S factor (Table 12) is used in the five experiments and the different scenarios considered. A large variability of results can be observed. If the p-value of the test is lower than some significance level (common choices are 0.10, 0.05, and 0.01), then there is statistically significant evidence that a trend is present in the time series data. So when these are below 0.1, the trends are considered to be significant.

Table 12. Sen's slope (S) for the different experiments and scenarios.

Experiment	ssp119	ssp126	ssp245	ssp370	ssp585
IPSL-CM6A-LR (FR)	-9510	-7228	-7673	-6230	-3295
EC-Earth-Veg-LR (EU)	-3932	-4302	174	471	5595
CAMS-CSM1-0 (CN)	-11808	-18194	-13841	-9073	-6061
GFDL-ESM4 (USA)	4621	8892	12674	5255	7622
MRI-ESM2-0 (JPN)	-10948	-477	-4719	3031	-801

To better visualise the trends, it was decided to group the data according to the proposed scenario and to plot them graphically (Fig. 12). In this way, a generalised decrease in the amount of monthly precipitation can be observed, in all cases except for ssp370 where a slight increase in the mean can be observed.

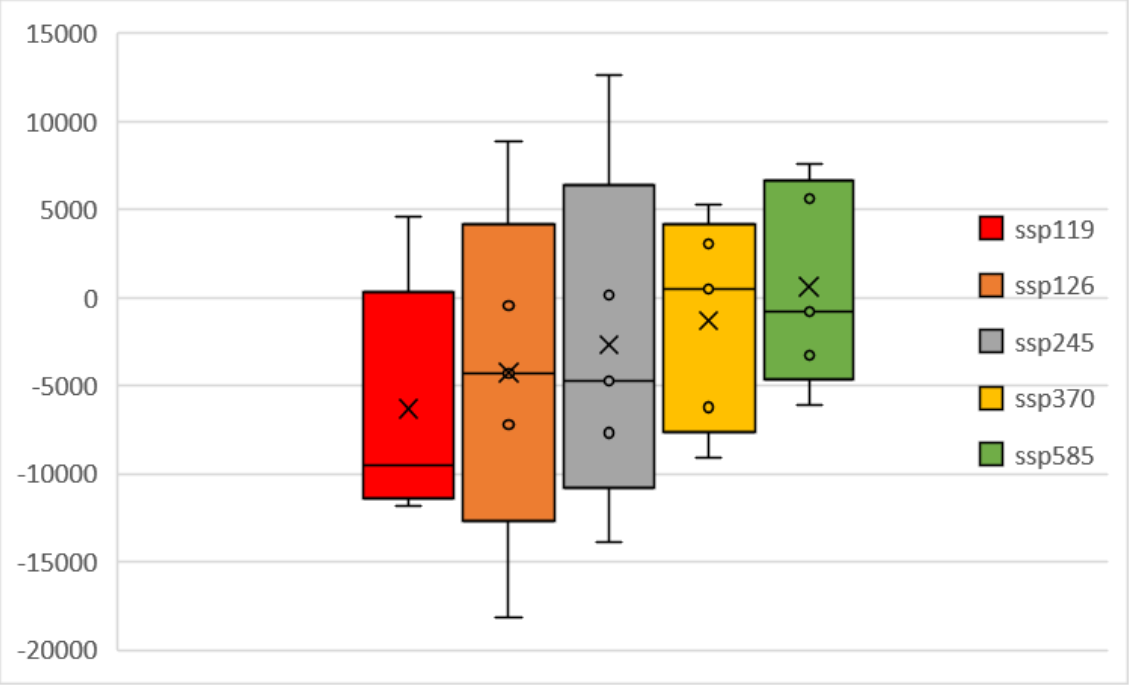

Figure 12. Graphical representation of Sen's slope (S) values for the different scenarios, with monthly data.

As a second case study, the Mann-Kendall trend analysis was performed for the seasonal rainfall data. In this case, the data was plotted by grouping the experiments but separating them into stations (Fig. 13). This makes it easier to observe trends.

The main difference that can be observed concerning the trend study by historical data is that in the case of summer, a decrease in precipitation is observed. This fact must be taken into account because it is in this season when the most intense rainfall occurs, which can put the integrity of the infrastructure at risk.

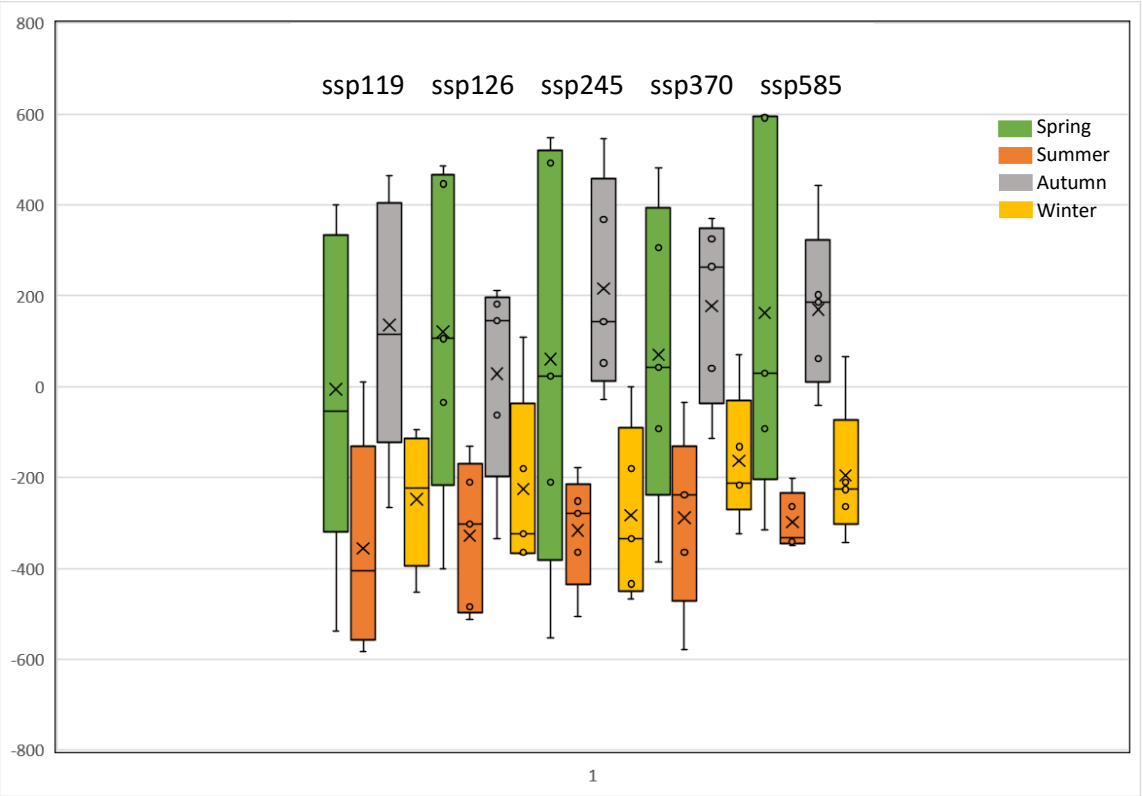

Figure 13. Graphical representation of Sen's slope (S) values for the different scenarios, with seasonal data.

5. Discussion

In the present thesis it is intended to analyse the climatic series, corresponding to the Bacanuchi station. For this purpose, the climatic series were analysed using the double mass curve method. The method allows effectively to detect changes of slope or displacements in the double mass curve so that corrections can be made in case these were necessary. Fortunately, this was not necessary and the homogeneity of the data could be checked by comparing the Bacanuchi station with the precipitation data obtained from the CHIRPS satellite database. This satellite data, after checking their compatibility with those obtained at the station, allow us to use a much broader and more complete time series for the study. In addition, the Bacanuchi station was compared with adjacent stations by applying the double mass method. By corroborating the homogeneity and compatibility of the climatic series, it can be confirmed that the data from the Bacanuchi station is representative of the upper basin of the Sonora River.

Several methods have been applied for the frequency analysis. The first was the Weibull method, which allowed us to obtain the annual exceedance values. The method of estimating rainfall amounts for selected probabilities serves to corroborate that the information obtained with the Weibull method is correct. Beyond this statement, it does not provide any new information. Therefore, it is a dispensable method for the study carried out. The next method, probability plot, provides us with information about the

distribution of annual rainfall. These are concentrated around the mean, the extremes being scarce. This is general information that does not add value to the study, so it is dispensable and can be obtained as a complementary result of another method. Next, the maximum daily precipitation data was analysed by the Gumbel method. This method gave us a wide range of return periods for the maximum precipitation. This is very useful information, as large rainfall events are the only ones that can cause a risk to the mine infrastructure. These are in the order of thousands of years, which means that it is very unlikely that an event of sufficient magnitude to put the infrastructure at risk would occur. The last method applied in this section was the IDF curves. This method allows us to observe the return periods for rainfall increases of one to five days. Although at first sight it seems to be very useful information, due to the small range of return periods (maximum 250 years), it does not provide useful information. This is due to the fact that data greater than a thousand year return period is necessary to have sufficiently intense rainfall to take them into account. On the contrary, in this study the maximum that was obtained was a rainfall that hardly exceeds 80 mm/day for a return period of 250 years. Although it is a good methodology, the time span it covers is insufficient for the magnitudes used in this study. On the other hand, the Gumbel method perfectly covers the shortcomings observed in the IDF curves method.

Following a frequency analysis, the data before the spillage was further analysed. According to the first reports provided by the mining company, this was an incident caused by extreme rainfall from Hurricane Odille. In order to verify the veracity of this statement, the heaviest rainfall before the spillage event was analysed. This was a rainfall of 87.2 mm over a time span of two days. After calculations for five different scenarios, it was found that in no case was the pre-spillage rainfall sufficient to cause a spill. For spillage to have occurred due to extreme rainfall, the rainfall would have to be 170 mm or more in one day (Table 13). Considering scenario 4 (chapter 4.3.), the only scenario in which sufficient runoff would be produced to exceed the maximum capacity of Bordo Poniente (120,000 m^3). This implies a return period of more than 3500 years according to the Gumbel method.

Tabe 13. Volumes in m^3, according to scenario 4 for different extreme rainfall events.

mm in 1 day	160	170	180	190	200
m3	119,299	124,255.2	129,211.4	134,167.5	139,123.7

A trend analysis was then performed for the number of extreme precipitation values and precipitation per season. In the first case a clear negative trend is observed, with the exception of two cases where a slight increase is seen, but too small to be relevant. This would indicate that the number of events would be reduced. Despite having a clear negative trend, this does not necessarily indicate that there is a reduction in annual precipitation, but rather that it may be spread over a smaller number of events. This would result in a greater torrential nature of extreme precipitation. The second case analysed is the one that corresponds to the trends in total rainfall per season. In this case, a decrease in rainfall is observed in all seasons except for those occurring in

summer. Summer is also the season with the highest rainfall. This case, in which the number of events decreases but summer rainfall increases, would mean that despite maintaining a similar amount of rainfall, an increase is of intense rainfall that could affect the mine's infrastructure is expected. This would increase the risk of affecting Bordo Poniente and the other BVC dams.

In the case of the future projections obtained from the Copernicus database (2023), these were processed using the statistical downscaling method (SDS), in order to homogenise the climate series of the different experiments with respect to the Bacanuchi data. Once the information was processed, the trend was analysed using the Mann-Kendal method. In the first case, the trends in monthly rainfall were analysed. The result was obtained was a great variability in trends, so that no conclusive results can be drawn from this approach. In spite of this general decrease in the amount of monthly precipitation in all cases except for ssp370 where can observed a slight increase can be observed in its mean. For the second case study, the same methodology was applied to the precipitation per station. In this case, a significant decrease in precipitation is observed in summer. This fact, contrary to the seasonal trend analysis with historical data, would imply a decrease in the heaviest rainfall. By reducing the heaviest rainfall, it can be said that the risk of affecting the BVC dams would be considerably reduced.

6. Conclusions

After compiling and checking the homogeneity of the climate series, it can be concluded that the correlation between weather station data and satellite data is compatible. Therefore, the data downloaded from CHIRPS can be used for the following procedures without any error. By comparing the Bacanuchi station with the others in the area, the data from the Bacanuchi station have been found to be representative of the region.

In the case of the pre-incident rainfall data, it can be concluded, after analysing the pre-spillage rainfall events, that they were not intense enough to cause damage to the mine infrastructure. Therefore, the spillage must have been the result of other factors.

In terms of extreme rainfall, a significant decrease in the number of episodes, both annually and seasonally, can be observed. The only exception is the slight increase in these episodes in summer, which is the season with the highest rainfall. Thus, it could be said that the probability of an extreme precipitation event with risk potential has increased. In any case, this should not be sufficient to cause a second spill.

When analysing the different scenarios for the future, a general decrease in summer rainfall has been observed. As these are the heaviest rainfalls, this implies a decrease in risk. Taking these factors into account, together with the construction of two additional dams of greater capacity, it can be concluded that it is practically impossible for rainfall to cause a spillage.

7. References

ARAUJO QUINTERO, G. G. (2017). Caracterización hidrogeológica de a subcuenca del Río Bacanuchi, Sonora, México.

Bürger, G. (1996). Expanded downscaling for generating local weather scenarios. Climate Research, 7(2), 111-128.

Climate Hazards Group (CHIRPS). Retired July 7, 2023 from http://chg.geog.ucsb.edu/data/chirps

CONAGUA (2023) Red de estaciones climatológicas. Servicio Meteorológico Nacional (SMN). Retrived June 26, 2023, from https://smn.conagua.gob.mx/es/

Copernicus Climate Change Service. (n.d.). Retrieved July 7, 2023 from https://climate.copernicus.eu

Dehn, M., & Buma, J. (1999). Modelling future landslide activity based on general circulation models. Geomorphology, 30(1-2), 175-187.

Dirk, R. A. E. S. (2013). Frequency analysis of rainfall data. College on Soil Physics—30th Anniversary (1983-2013), The Abdus Salam International Centre for Theoretical Physics, 210-244.

Fajardo Calzada, J. L. (2016). Modelación conjunta de los recursos hídricos superficiales y subterráneos de la cuenca alta del Río Sonora.

Fowler, H. J., Blenkinsop, S., & Tebaldi, C. (2007). Linking climate change modelling to impacts studies: recent advances in downscaling techniques for hydrological modelling. International Journal of Climatology: A Journal of the Royal Meteorological Society, 27(12), 1547-1578.

García, E. (2004). Modificaciones al sistema de clasificación climática de Köppen. Universidad Nacional Autónoma de México.

García Romero, A. N. (2022) Síntesis, análisis e interpretación de la información publicada sobre el derrame de unos 40,000 m3 de solución ácida ferro-cuprífera de la Mina Buenavista del Cobre.

Huth, R. (1999). Testing for trends in data unevenly distributed in time. Theoretical and Applied Climatology, 64, 151-162.

IPCC (2007): Climate change the physical science basis. In Agu fall meeting abstracts (Vol. 2007, pp. U43D-01).

Infante Blanco, E.(1998) Introduccion al estudio hidrogeografico y balance hidrologico de la cuenca del Rio Sonora hasta la Estacion Hidrometrica El Oregano.

Instituto Nacional de Estadística y Geografía (México) (2017). Estudio de información integrada de la Cuenca Río Sonora y otras / Instituto Nacional de Estadística y Geografía.-- México : INEGI, c2017. 92p. ISBN 978-607-530-011-5.

Karl, T. R., Wang, W. C., Schlesinger, M. E., Knight, R. W., & Portman, D. (1990). A method of relating general circulation model simulated climate to the observed local climate. Part I: Seasonal statistics. Journal of Climate, 3(10), 1053-1079.

Kendall, K. (1975). Thin-film peeling-the elastic term. Journal of Physics D: Applied Physics, 8(13), 1449.

King, R. E. (1939). Geological reconnaissance in northern Sierra Madre occidental of Mexico. Bulletin of the Geological Society of America, 50(11), 1625-1722.

Kohler, M. A. (1949). On the use of double-mass analysis for testing the consistency of meteorological records and for making required adjustments. Bulletin of the American Meteorological Society, 30(5), 188-195.

Loukas, A., Vasiliades, L., & Tzabiras, J. (2008). Climate change effects on drought severity. Advances in Geosciences, 17, 23-29.

Mann, H. B. (1945). Nonparametric tests against trend. Econometrica: Journal of the econometric society, 245-259.

McLeod, A. I., & Hipel, K. W. (1994). Tests for monotonic trend. In Stochastic and Statistical Methods in Hydrology and Environmental Engineering: Time Series Analysis in Hydrology and Environmental Engineering (pp. 245-270). Dordrecht: Springer Netherlands.

NAVARRO APODACA, A. Z. (2009). Evaluación hidrológica superficial de la cuenca del río Sonora.

O'Neill, B. C., Tebaldi, C., Van Vuuren, D. P., Eyring, V., Friedlingstein, P., Hurtt, G., ... & Sanderson, B. M. (2016). The scenario model intercomparison project (ScenarioMIP) for CMIP6. Geoscientific Model Development, 9(9), 3461-3482.

Salas, J. D. (1993). ‘‘Analysis and modeling of hydrologic time series.’’Handbook of hydrology, D. R. Maidment, ed., Chapter 19, McGrawHill, New York

SIATL: Simulador de Flujos de Agua de Cuencas Hidrográficas. http://antares.inegi.org.mx/analisis/red_hidro/SIATL/#

Vasiliades, L., Loukas, A., & Patsonas, G. (2009). Evaluation of a statistical downscaling procedure for the estimation of climate change impacts on droughts. Natural Hazards and Earth System Sciences, 9(3), 879-894.

Von Storch, H.: On the use of “inflation” in statistical downscaling,J. Climate, 12, 3505–3506, 1999.

Wilby, R. L., & Wigley, T. M. (1997). Downscaling general circulation model output: a review of methods and limitations. Progress in physical geography, 21(4), 530-548.

Xu, C. Y. (1999). From GCMs to river flow: a review of downscaling methods and hydrologic modelling approaches. Progress in physical Geography, 23(2), 229-249.

Xu, C. Y., Widén, E., & Halldin, S. (2005). Modelling hydrological consequences of climate change—progress and challenges. Advances in Atmospheric Sciences, 22, 789-797.

Yocupico-Anaya, M. T. y Gómez-Álvarez, A., (1987). Estudio de la Contaminación por Metales Pesados en el Río Sonora y su efluente el Río Bacanuchi. Tesis profesional UNISON. Hermosillo, Sonora

Yue, S., Pilon, P., & Cavadias, G. (2002). Power of the Mann–Kendall and Spearman's rho tests for detecting monotonic trends in hydrological series. Journal of hydrology, 259(1-4), 254-271.

Annex I

This annex shows the graphs produced as a result of the trend analysis using the Mann-Kendall method. These correspond to the period 1981-2022. In the first case, extreme rainfall values for cumulative rainfall of one to five days are considered to show the trend. These are classified depending on the intensity and number of events of this magnitude for the time period described. The second case shows the trend variation, depending on the rainfall produced in the same season per year.

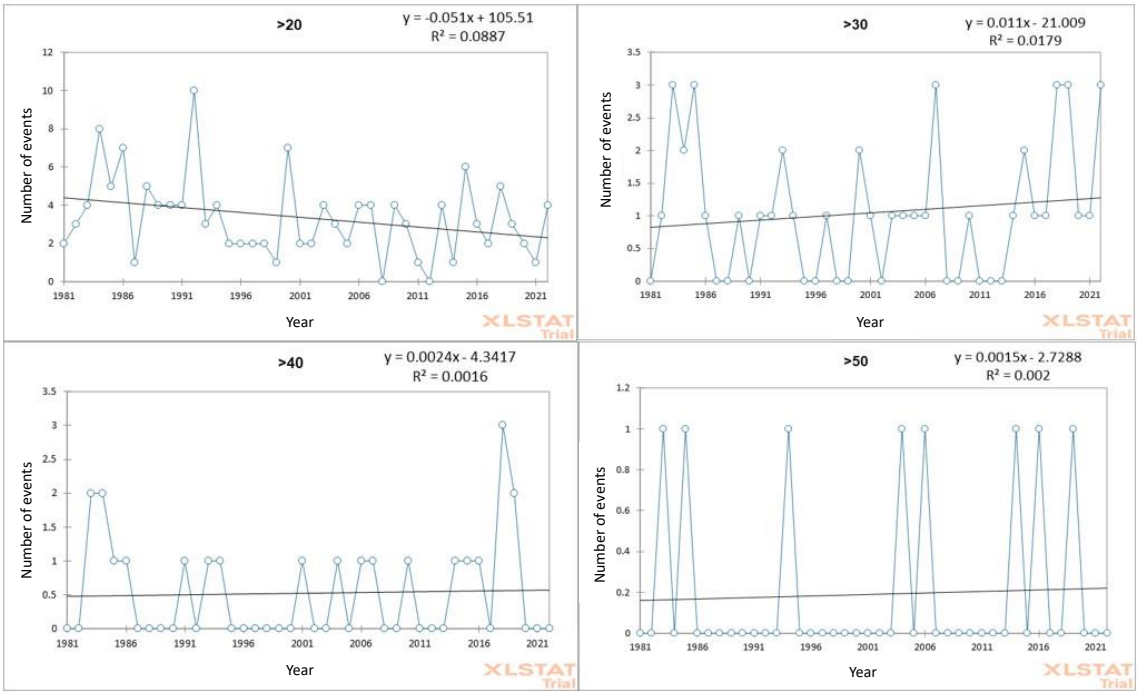

Figure showing the trend variations according to the number of days of extreme rainfall produced annually, for the years 1981-2022. This figure considers the time period of 1 day of accumulated rainfall.

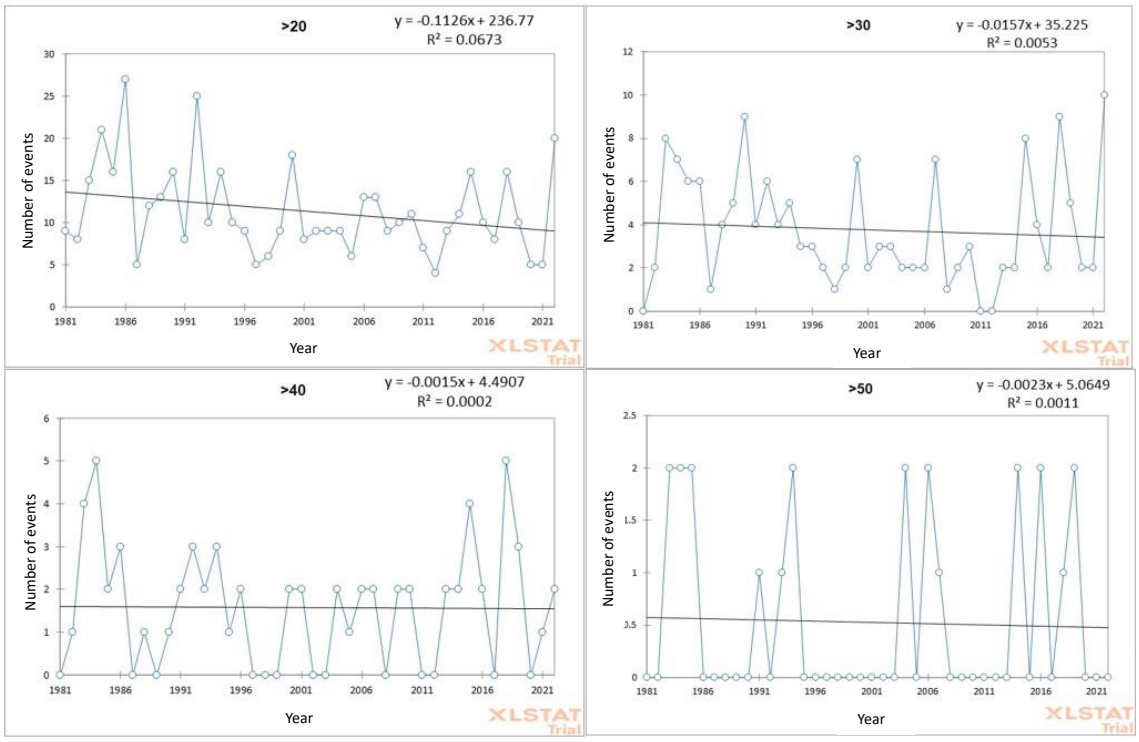

Figure showing the trend variations according to the number of days of extreme rainfall produced annually, for the years 1981-2022. This figure considers the time period of 2 days of accumulated rainfall.

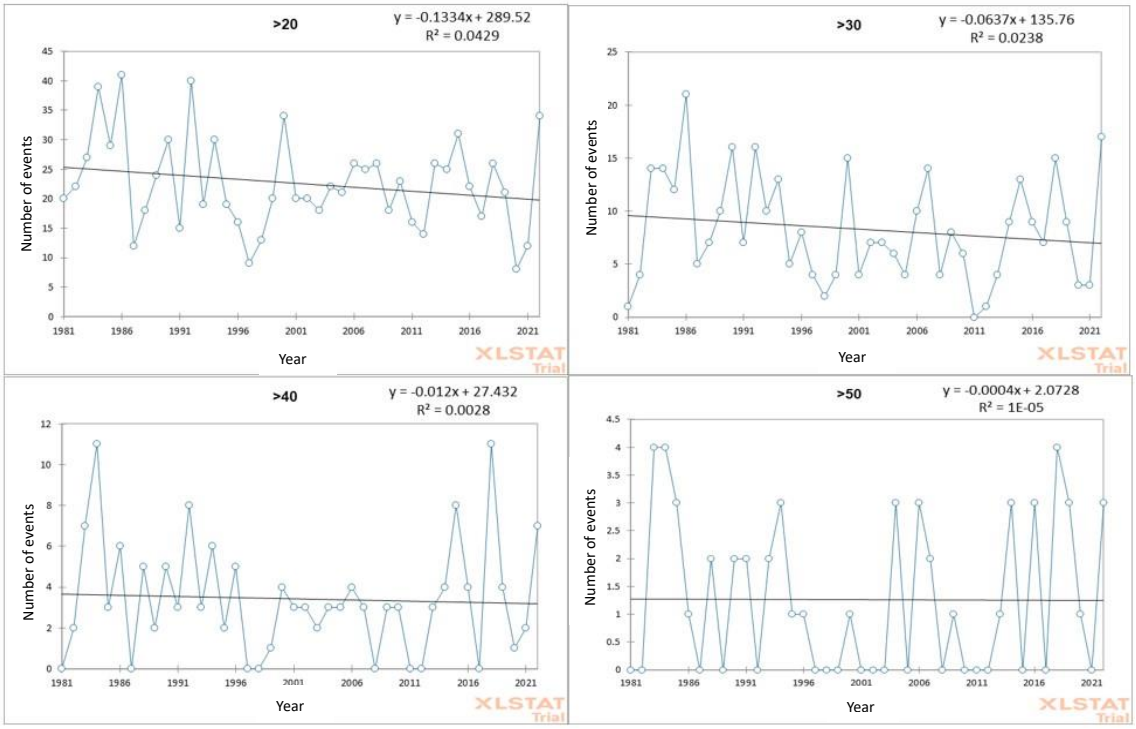

Figure showing the trend variations according to the number of days of extreme rainfall produced annually, for the years 1981-2022. This figure considers the time period of 3 days of accumulated rainfall.

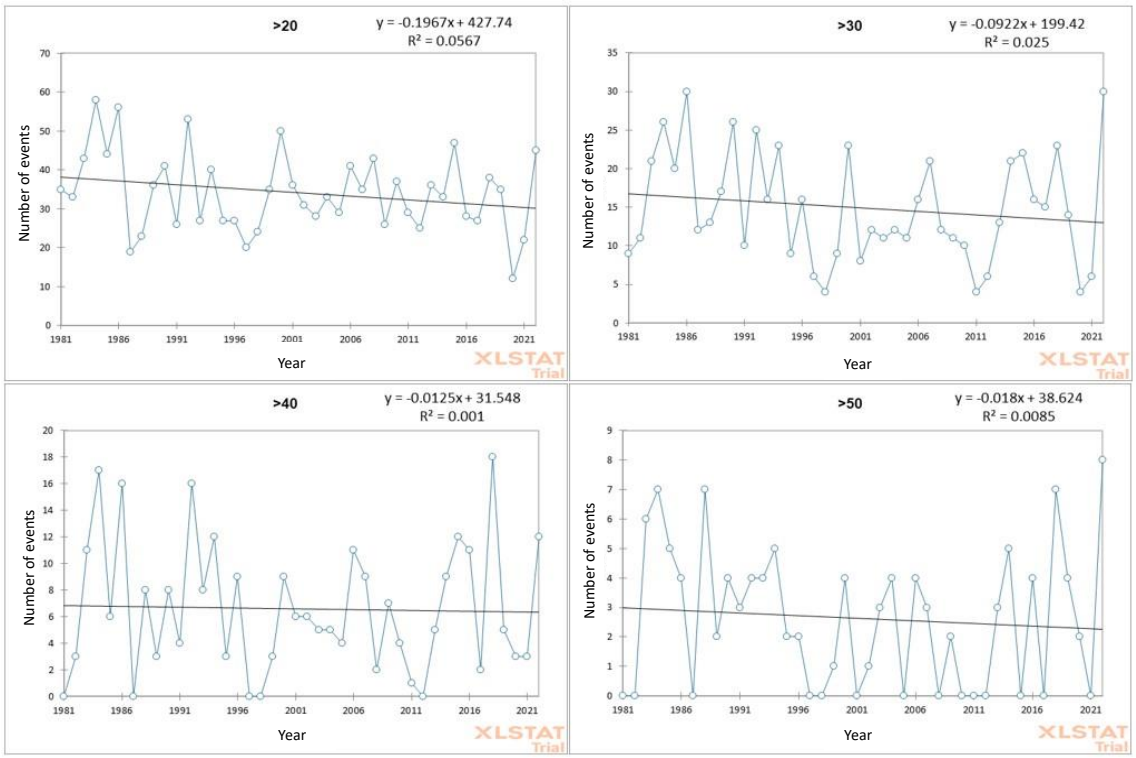

Figure showing the trend variations according to the number of days of extreme rainfall produced annually, for the years 1981-2022. This figure considers the time period of 4 days of accumulated rainfall.

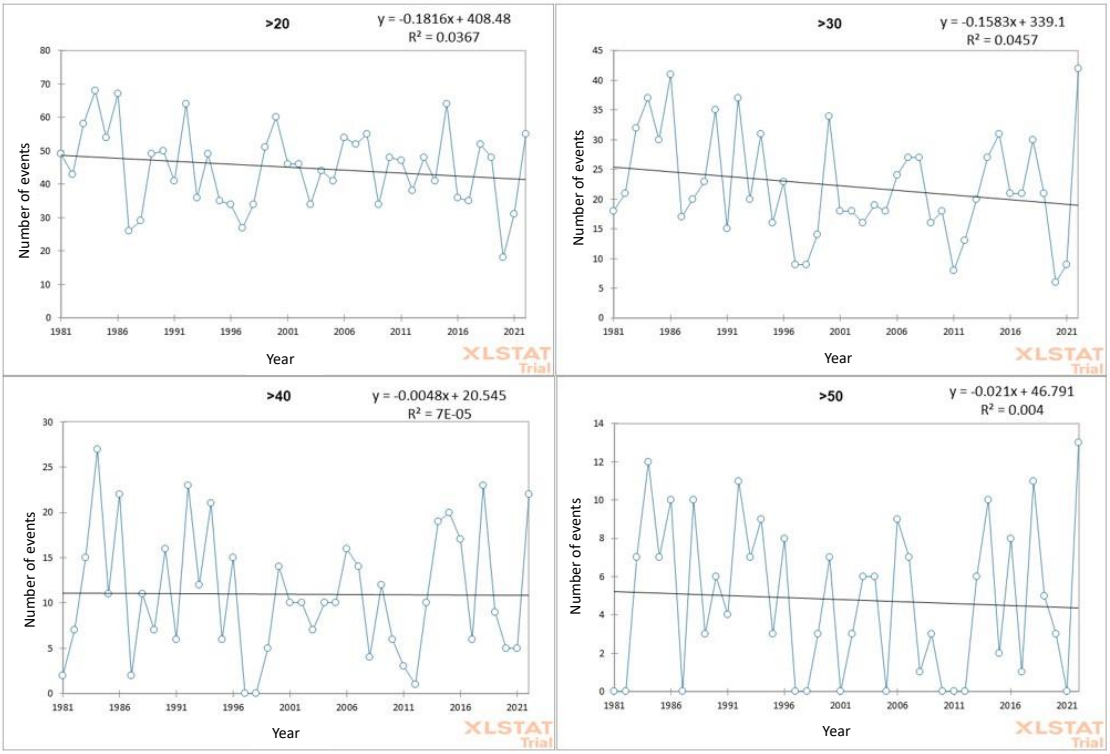

Figure showing the trend variations according to the number of days of extreme rainfall produced annually, for the years 1981-2022. This figure considers the time period of 5 days of accumulated rainfall.

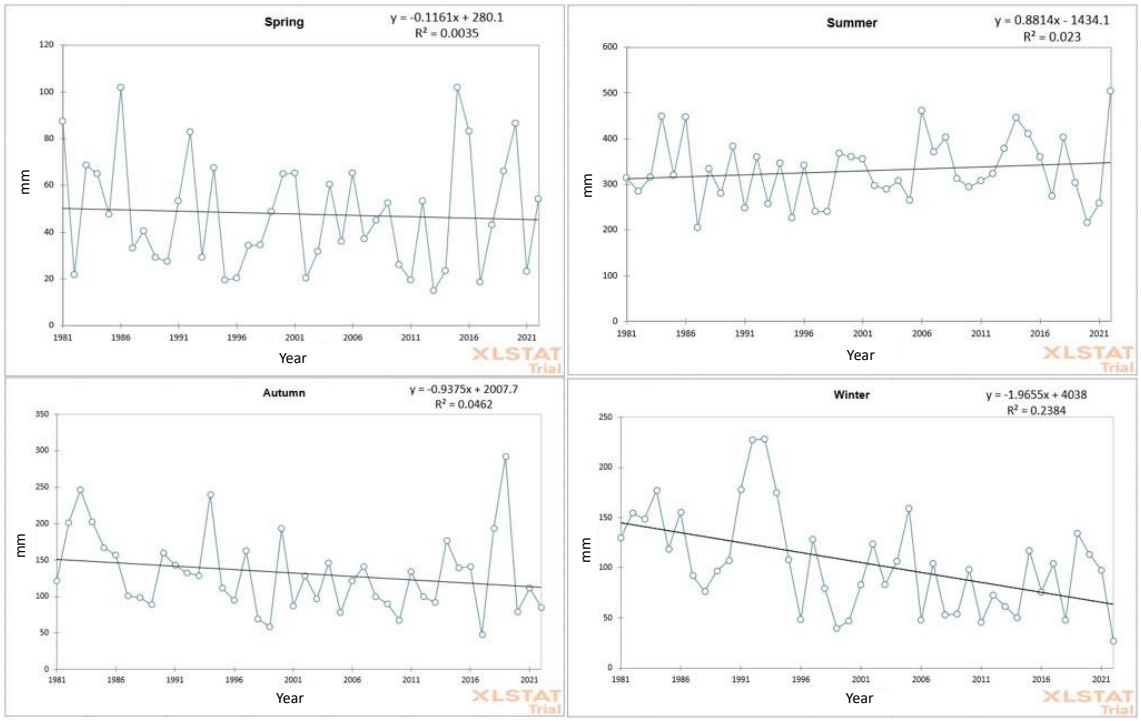

Figure showing the trend variations according to the seasons, for the rainfall the years 1981-2022.